DEGREE PROJECT

A comparison of boulder morphology in the two geologic units of asteroid (101955) Bennu

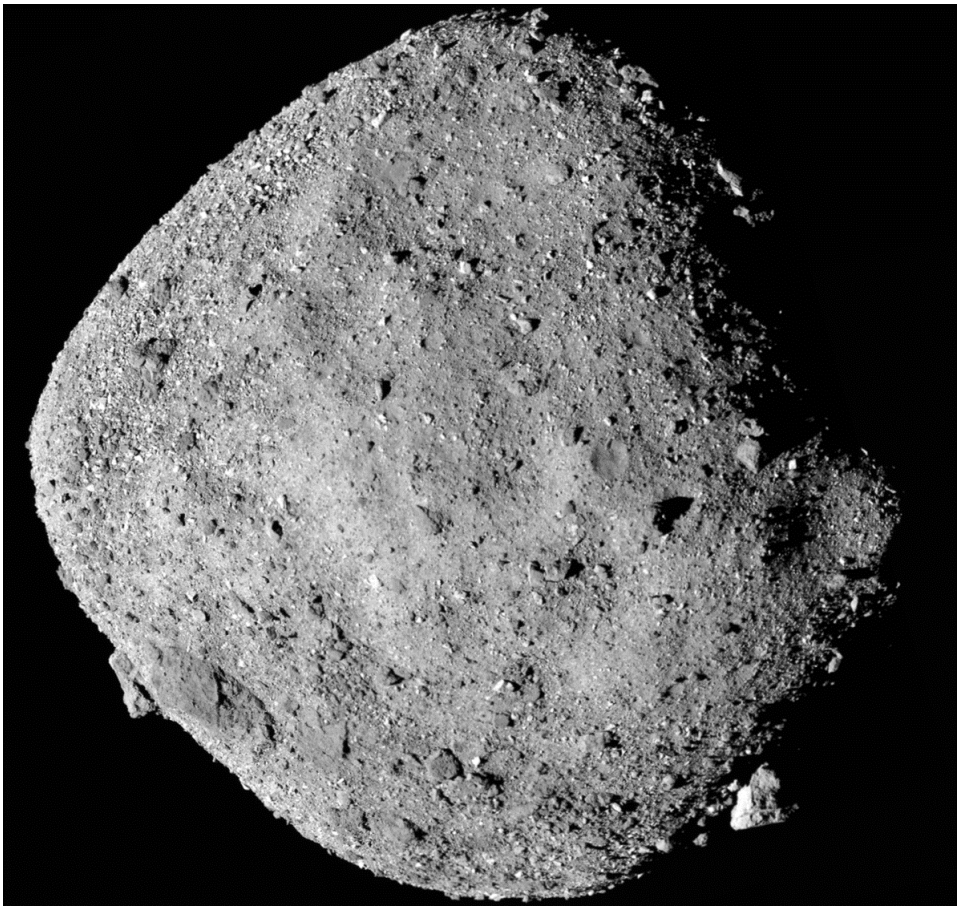

Evelina Svanström

Space Engineering, master's level
2024

Luleå University of Technology
Department of Computer Science, Electrical and Space Engineering

LULEÅ UNIVERSITY OF TECHNOLOGY

[This page intentionally left blank]

Abstract

NASA's Origins, Spectral Interpretation, Resource Identification, and Security-Regolith Explorer (OSIRIS-REx) spacecraft arrived at the near-Earth rubble pile asteroid (101955) Bennu in December 2018, where it took high resolution images of the surface. The images revealed that the surface is covered with boulders of various sizes. The morphology of these boulders can provide valuable information about the body's history and the mechanical properties of the regolith. In this work, I use OSIRIS-REx images to map the outline of boulders on Bennu in two different geologic units: a Rugged Unit and a Smooth Unit. The two units are differentiated by surface texture, shape features and geologic features. This work was implemented using the open-source software QGIS. I compare the two units' boulder morphology firstly in terms of boulder roughness by looking at the shape factors solidity (to what extent a boulder's area equals that of its convex hull area) and circularity (to what extent a boulder's perimeter is similar to the circumference of a circle with the same area). Then I study boulder compactness, by looking at the shape factors elongation (the ratio between its minor and major axis) and roundness (to what extent a boulder's area resembles that of a circle enclosing the boulder). Despite the geologic differences, I find that there is no significant difference in the boulder roughness and compactness between the two units. Both regions' boulders possess a large variation of values that overlap significantly. My results match well with laboratory impact experiments, implying that the regolith was created by a catastrophic impact, which is in agreement with Bennu's status as a rubble-pile asteroid. I also find that the Smooth Unit tends to have smaller boulders (0.579 ± 0.35 m) with more boulders mapped (total 2426) than the Rugged Unit (0.711 ± 0.48 m, total 1774 boulders mapped). Finally, I show that smaller boulders tend to be rounder and less rough than larger boulders in both units. My results imply that boulder morphology is relatively uniform over the surface of Bennu, also indicating that the mechanical material properties associated with the boulder shape (such as for example tensile strength of the assembly, bulk porosity and formation history) are similar in the two units. Although the units are geologically distinct, the boulder morphology is homogeneous.

Contents

List of Figures

List of Tables

Abbreviations

DART	Double Asteroid Redirection Test
K-Pg	Cretaceous-Paleogen
NASA	National Aeronautics and Space Administration
NEA	Near Earth Asteroid
OCAMS	OSIRIS-REx Camera Suite
OLA	OSIRIS-REx Laser Altimeter
OSIRIS-REx	Origins, Spectral Interpretation, Resource Identification and Security-Regolith Explorer
OTES	OSIRIS-REx Thermal Emission Spectrometer
OVIRS	OSIRIS-REx Visible and Infrared Spectrometer
PDS	Planetary Data System
QGIS	Quantum Geographic Information System
REXIS	Regolith X-ray Imaging Spectrometer
TAG	Touch-And-Go
TAGSAM	Touch-And-Go Sample Acquisition Mechanism

Nomenclature

A	Area of boulder (m^2)
P	Perimeter of boulder (m)
a	Major axis of boulder (m)
b	Minor axis of boulder (m)
H	Convex hull area (m^2)
r_1	Radius of circle with the same perimeter as boulder (m)
A_1	Area of circle with the same perimeter as boulder (m^2)
A_2	Area of minimum circumscribed circle (m^2)
C	Circularity (1)
E	Elongation (1)
S	Solidity (1)
R	Roundness (1)
α	Angle of shadows in the image (°)
β	Angle of boulder orientation (°)

1 Motivation

There are many unknown questions about our planet and our Solar System. The early phases of the creation of the Solar System and Earth, how we got water on Earth, and how life developed on Earth are questions we only have theories about. A step towards better understanding these questions is to study asteroids.

Asteroids are remnants from the early formation of the Solar System, so they can teach us about how it formed and what the conditions were back then. Past collisions of asteroids with Earth likely also delivered carbon-based molecules and volatile materials that led to the creation of water and subsequently the evolution of life on our planet. They were also important when they collided with Earth, which significantly altered our biosphere, which was for example seen at the Cretaceous-Paleogene (K-Pg) extinction event 66 million years ago [21]: The K-Pg extinction is believed to have been caused by a 10 to 15 km large asteroid [21]. Asteroids with an orbit close to Earth are called Near Earth Asteroids (NEAs). The abundance of NEAs and the potential harm they would have to life on Earth has led to a great interest in asteroids, including asteroid deflection missions, such as NASA's Double Asteroid Redirection Test (DART) mission, which redirected an asteroid's orbit with the help of a kinetic impact [7]. Lastly, a more recent interest in asteroids is their potential as a way of mining valuable resources that could be brought back to Earth [38].

Rubble-pile asteroids are a type of asteroids that originate from a catastrophic disruption of one or more parent bodies. When the parent-body is disrupted the rubble pieces reassemble due to gravity, forming an asteroid of relatively low density and with a surface covered in boulders [16]. This surface material is called regolith (from Greek rhegos - blanket and lithos - rock). Boulders can also be generated as ejecta of less violent impacts [24]. Studying the boulders found on the surface of asteroids can give us insight into the body's collisional history and geological evolution, as well as telling us about the mechanical properties of the body's regolith [33]. The Near Earth asteroid (101955) Bennu is one of these rubble-pile asteroids [19]. It was visited by NASA's sample-return mission Origins, Spectral Interpretation, Resource Identification and Security-Regolith Explorer (OSIRIS-REx), which arrived in December 2018 [20]. OSIRIS-REx took high resolution images of the surface of Bennu. In this thesis I use these images to study boulder morphology on asteroid Bennu. In the context of my thesis, boulder morphology refers to the shape (i.e. the two-dimensional outline) and size of boulders, found by studying images, which can be used to gain valuable information

about Bennu.

The main goal of my thesis is to assess the difference in boulder morphology between two geologic units on the asteroid Bennu previously identified by Jawin et al. (2022) [14]: An older Smooth Unit and a comparatively younger Rugged Unit. By comparing the boulder morphology of these two units, I aim to establish the homogeneity of Bennu's regolith, and determine whether resurfacing and/or erosive possesses play a part in altering the the geology of the asteroid. To set my work further into context, I also compare my results with studies of other bodies (the asteroids Ryugu, Itokawa, and Eros, the comet 67P/Churyumov–Gerasimenko and Mars) and laboratory experiments.

2 Introduction and Background

2.1 Asteroids

Asteroids are a fascinating subject to study as they are remnants of the creation of our solar system. They are made up from the material in the early stages of the formation of the solar system that did not get absorbed into the Sun or planets.

Asteroids are small bodies that orbit the Sun, that are not comets, moons or natural satellites. Most asteroids are found in the so called Asteroid Belt between Mars and Jupiter. Asteroids are called Near-Earth Asteroids (NEAs) when they have orbits that pass close by or cross the Earth's orbit. The NEAs are further categorized based on the perihelia and aphelia of their orbits: **Amor** asteroids' orbits approach Earth's orbit but do not cross it, **Apollo** asteroids have orbits that cross Earth's orbit but spend most of their orbit outside of it, **Aten** asteroids have their aphelia greater than Earth's perihelion so they spend most of their orbit inside of Earth's orbit, and finally **Atira** asteroids, which have their orbits completely inside of Earth's orbit [21].

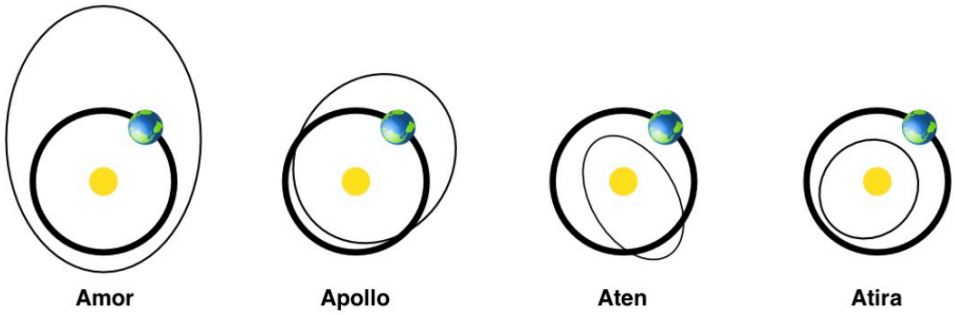

Figure 1: An illustration of the different categories of Near Earth Asteroids [25].

Asteroids' radius can range from between a few meters to hundreds of kilometers. They can either be a single, large rock (monolithic), or a collection of rocks held together by a weak gravity, so-called rubble-pile asteroids. Rubble-pile asteroids are believed to be the most common kind, especially for the 200 m to 10 km size range [16]. Rubble-pile asteroids are created when one or more parent bodies disrupt due to an impact, and the pieces then reassemble due to self-gravity [16]. Asteroids can also be divided into spectral classes relating to their compositions. The main classes include carbonaceous, siliceous and metallic asteroids [3].

2.2 (101955) Bennu

Asteroid (101955) Bennu is a potentially hazardous Near Earth Asteroid in the Apollo group. An image of Bennu can be seen in Figure 2. Bennu is a relatively uncommon carbonaceous rubble-pile asteroid that was discovered on the 11th of September 1999 [19]. It was originally known as 1999 RQ36. The asteroid has a diameter of around 490 meters [20], and an orbital period of 1.20 Earth years [13]. A sketch of Bennu's orbit can be found in Figure 3. As it is a rubble-pile, it was created by a catastrophic impact that broke up its parent body, and the rubble pieces then reassembled due to gravity. This structure and its composition causes it to have a relatively low density of approximately (1.190 ± 13) kg/m^3 [20]. It is also a very dark object, with an albedo of 4.4% [20]. The asteroid also exhibits episodes of particle ejections from the surface, which was an unexpected surprise when it was first visited by a spacecraft [17]. A summary of Bennu's characteristics can be found in Table 1.

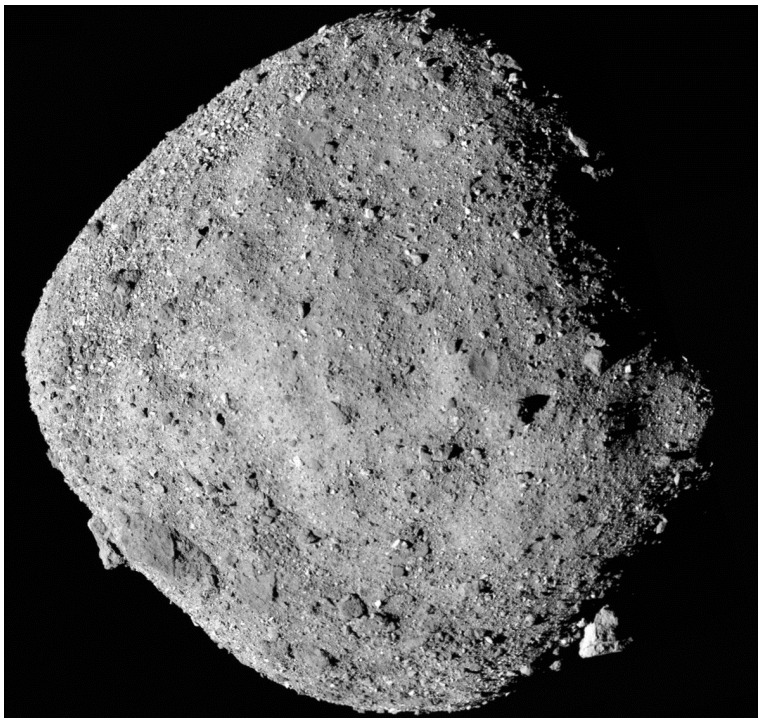

Figure 2: An image of Bennu [6].

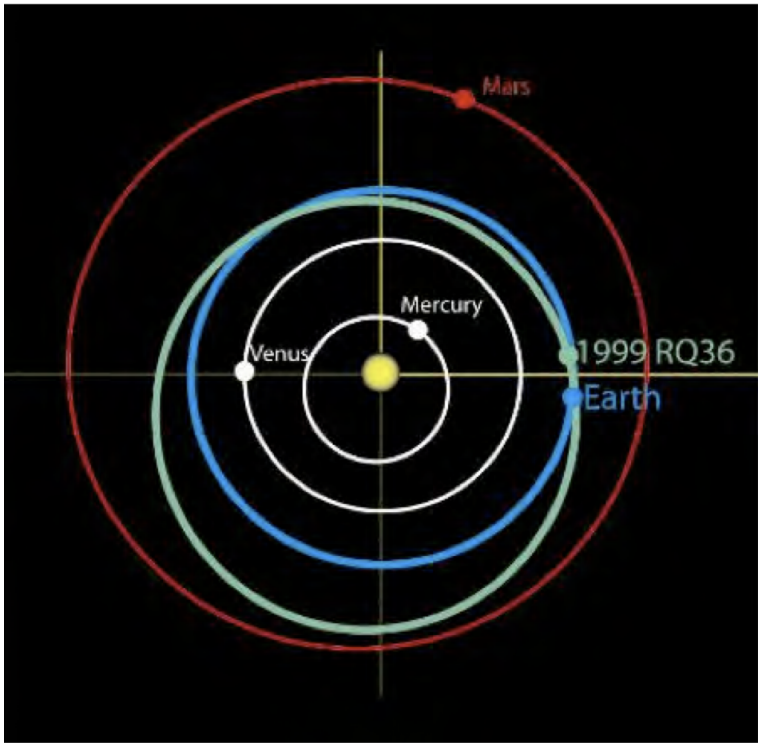

Figure 3: A sketch of Bennu's (1999 RQ36) orbit, drawn in green. Image from [13].

Table 1: Summary of Bennu's characteristics

Type:	Carbonaceous rubble-pile
Date of discovery:	11th September 1999
Diameter:	490 m
Orbital period:	1.20 Earth years
Density:	(1.190 ± 13) kg/m^3
Albedo:	4.4 %

Bennu is expected to have migrated from the Main Asteroid Belt and become a NEA around 1.75 ± 0.75 million years ago [1]. However, some surface features, such as craters, on Bennu are believed to be between 100 million and 1 billion years old [36], which means that the surface of Bennu can also give insight into the asteroid's time in the Main Asteroid Belt. Asteroids such as Bennu could potentially be the objects that brought prebiotic molecules and volatiles to Earth [20], making them interesting to study in the context of life's evolution on Earth.

2.2.1 Bennu's Geological Units

Jawin et al. (2022) identified two geological surface units on asteroid Bennu, one Smooth Unit and one Rugged Unit [14]. They separated these two regions by identifying the asteroid's surface texture, shape features (the equatorial bulge, longitudinal ridges, and troughs between the ridges) and geologic features (craters, boulders, etc.), by studying two global mosaics based on the OSIRIS-REx Camera Suite (OCAMS) images from the Approach and Detailed Survey mission phases, and the map from the OSIRIS-REx Laser Altimeter (OLA) [14].

The surface texture map was created by identifying two distinct regions with different surface texture when studying the mosaics [14]. The first region was identified as regions with smooth surface texture that did not contain many boulders at the given image resolution of 5 cm/pixel for one of the mosaics and 40 cm/pixel for the other mosaic. The other region was identified as regions with rugged surface texture and many boulders. This map can be found in Figure 4a.

For the shape feature map, they identified three main topographic shape features on Bennu: the equatorial bulge, longitudinal ridges, and troughs between the longitudinal ridges [14]. They found that the equatorial bulge and the longitudinal ridges were higher-lying than the troughs between them with the help of facet radius maps. They then mapped the high-lying regions (regions of locally higher altitude than 50 meters), and found that they corresponded to the ridges. The facet radius maps were derived from OLA. The troughs were then found to be the low-lying regions between the high-standing regions of the ridges. This map can be found in Figure 4b.

Geological features mapped by Jawin et al. (2022) in the geological features map include craters, lineaments, boulders, features caused by mass movement and particle ejection source regions [14]. The craters included were larger than 10 meters. Lineaments refers to different morphological features with linear alignments, such as ridges and scarps. They included lineaments longer than 100 meters. Boulders larger than 20 meters were also mapped as well as mass movement features, referring to morphologies of regolith and rocks that are related to mass movements. Lastly, particle ejection source regions were included. These were based on images taken by the navigation camera onboard OSIRIS-REx during particle ejection events. The geological features were identified with the help of OCAMS images and verified with the help of maps from OLA. This map can be found in Figure 4c.

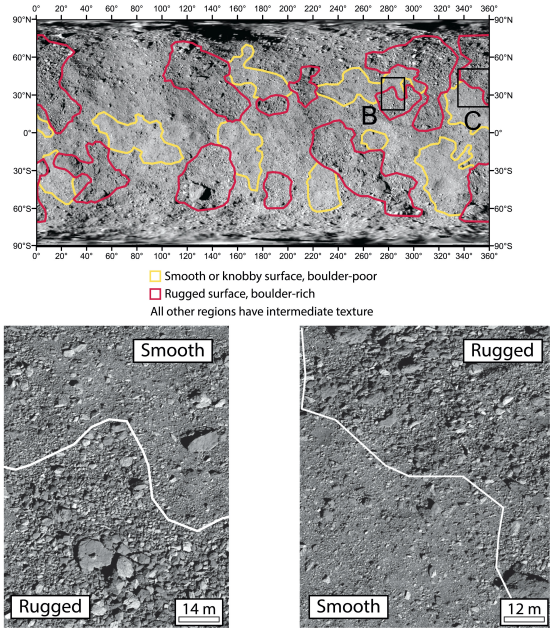

(a) Map of surface texture features

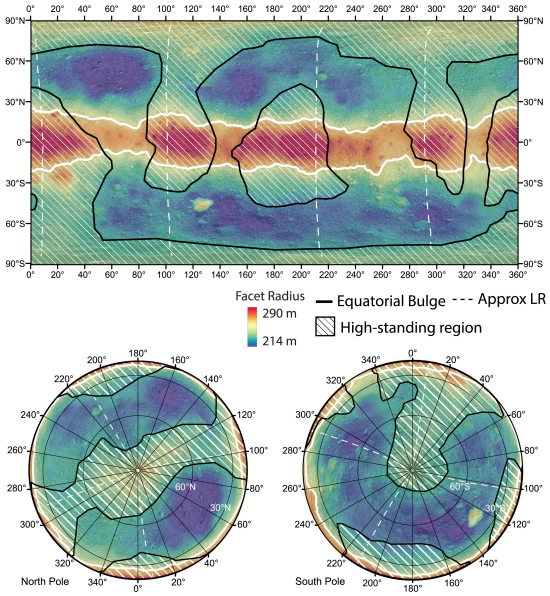

(b) Map of shape features

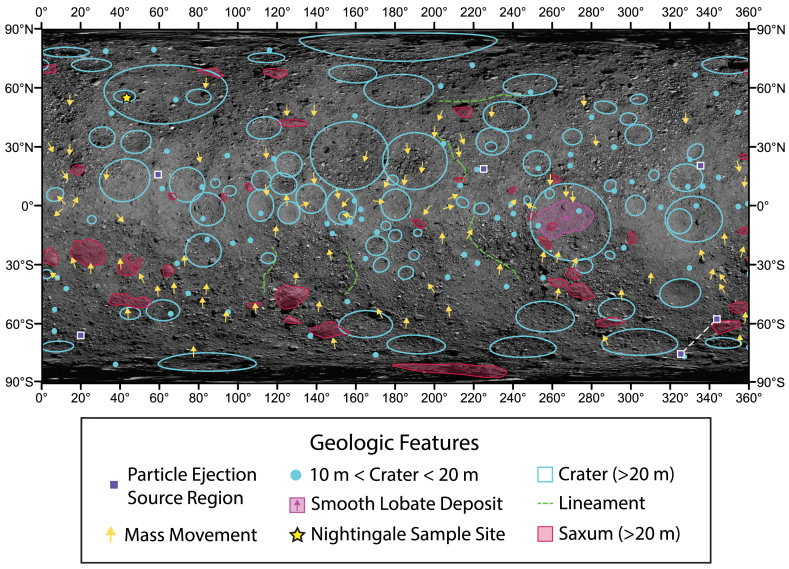

(c) Map of geological features

Figure 4: The three maps of surface texture features, shape features and geological features that were used to define Bennu's two geological units by Jawin et al. (2022) [14]

These three components (surface texture, shape features and geologic features) were mapped separately in both 2D and 3D, and then used to identify the two different geologic units [14]. In all three maps, they identified regional variations, and outlined broader regions with the same characteristics in all three (e.g. smooth texture in the texture map and low

concentration of geologic features in the geological features map). In that way, they were able to identify broader regions that had the same characteristics in all three maps, and by combining the three maps, they identified the two geologic units shown in Figure 5. However, it was the surface texture map that was the most distinctly different between the two units.

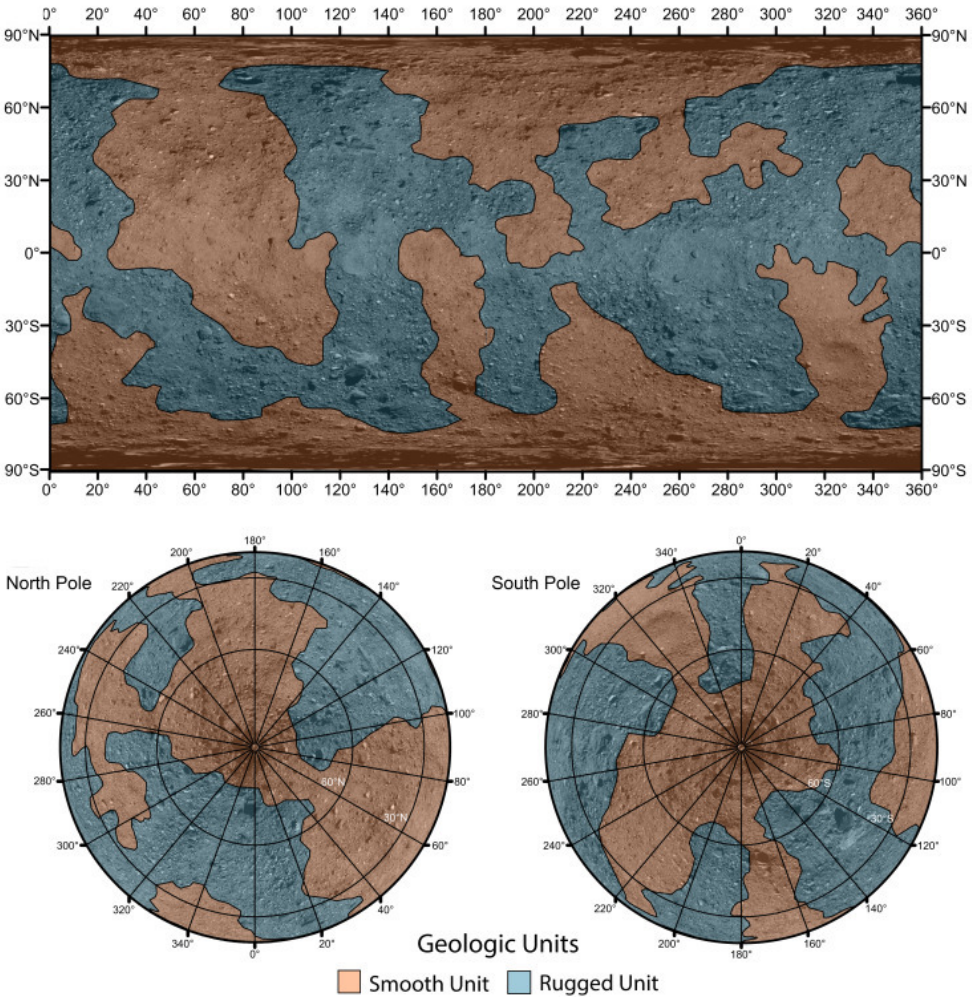

Figure 5: Bennu's two geological units as identified by Jawin et al. (2022) [14]

Based on the stratigraphy and the abundance of geological features that occur over time such as craters, the Rugged Unit is likely younger, and has resurfaced within in the past 0.5 Myrs, while the Smooth Unit is likely older and has not resurfaced within the past 2 MYr [14]. This means that the Smooth Unit is likely similar to how it looked when Bennu was still in the Main Asteroid Belt. However, something to keep in mind when studying boulders in these two regions is that resurfacing age is not the same as boulder age. Resurfacing age refers to when boulders get exposed to the surface, but the actual age of the boulder can be older.

In this thesis, I compare the boulder morphology in the two different geologic regions to see whether or not boulder morphology is influenced by the geologic setting.

2.2.2 Boulder Morphology

Boulder morphology has proven an important parameter in planetary science as it enables us to constrain the mechanical properties of a body's regolith [31]. For example, the roughness of a particle surface influences the internal friction of a particle assembly. Rougher, more angular particles will have higher internal friction than smooth, spherical particles. This generates a higher angle of repose and tensile strength of the particle assembly [12, 33]. Size segregation, sphericity, elongation and roundness can all be used to help determine past transport processes, as it has been observed on Mars [37]. Furthermore, as rubble-pile asteroids are made up of boulders, studying their size frequency distribution can teach us about the bulk porosity of the asteroid [11]. Boulder morphology can also help us better understand the formation of asteroids, for example as a result of impacts, that produce specific boulder elongations [24]. On Bennu, the surface boulder texture is also influenced by thermal cycling and micrometeorite impacts, however, it is unclear how exactly these combined processes relate to boulder morphology [26].

On Bennu, boulders have been used to infer the age of the asteroid (combined with other geologic features) [1, 36] and to study how the movement of them creates terraces [2], as well as recent mass movements on the surface [15]. Fractures on Bennu's boulders have also been studied to gain insights into how the surface has developed due to thermal weathering [10]. Bennu's boulders have also been used to date resurfacing events [14].

2.3 OSIRIS-REx

Origins, Spectral Interpretation, Resource Identification and Security-Regolith Explorer (OSIRIS-REx) is an asteroid sample-return mission by the National Aeronautics and Space Administration (NASA) [19]. An illustration of the OSIRIS-REx spacecraft can be seen in Figure 6. It was NASA's first sample-return asteroid mission, and its destination was the asteroid Bennu. It launched in September 2016 and reached Bennu in December 2018 [18]. The primary science goal of OSIRIS-REx was to return a pristine, carbon-rich regolith sample from the asteroid Bennu to Earth of at least 60 grams. Its secondary science goals included providing a global data set of the asteroid in order to be able to map its global properties, documenting the sample site at high resolutions, studying the Yarkovsky effect [19], and finally improving

asteroid astronomy by allowing comparison of the measurements from the spacecraft with ground-based observations [19].

Figure 6: An illustration of the OSIRIS-REx spacecraft above the surface of Bennu [6].

When the team decided which asteroid would be the target for OSIRIS-REx, they had over 500 000 identified asteroids to choose from. From these 500 000, over 7000 were in a Near Earth orbit. From these 7000, 192 had orbits that fulfilled the orbit-constraints for the mission to be successful. The team needed an asteroid that had a diameter of more than 200 meters, as smaller asteroids often have fast rotation rates and exhibit tumbling, which would make the sample collection manoeuvre more difficult. They identified 26 asteroids with a diameter larger than 200 meters. Of these 26, only 5 were thought to be carbon-rich based on spectral profiles. They wanted to return a sample that was pristine (has not been altered by other processes since its formation) and carbon-rich, as this is the kind of sample that can give us valuable information about the early stages of planetary formation. Of these 5 asteroids, Bennu was the one that was most extensively studied, both from the ground and space, so many parameters such as size, shape and rotation state were already known. This is why the team chose Bennu as their target asteroid [19]. A visualization of the selection process can be seen in Figure 7.

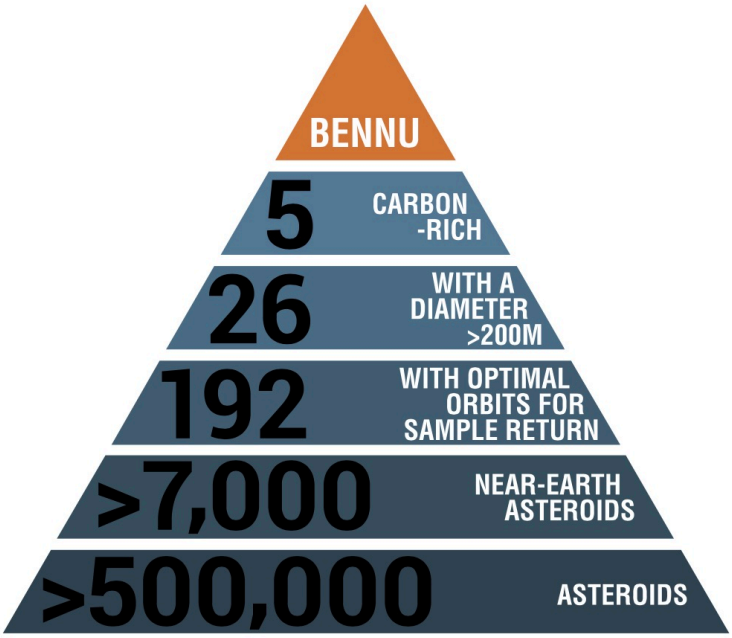

Figure 7: The selection process for choosing Bennu as the target asteroid of OSIRIS-REx. Image from [19].

OSIRIS-REx's scientific instruments included the OSIRIS-REx Laser Altimeter (OLA), the OSIRIS-REx Thermal Emission Spectrometer (OTES), the OSIRIS-REx Visible and Infrared Spectrometer (OVIRS), the Regolith X-ray Imaging Spectrometer (REXIS), and finally the OSIRIS-REx Camera Suite (OCAMS) [19]. It is the images taken by OCAMS that I have studied for this thesis. OCAMS was equipped with three different cameras: MapCam, SamCam, and PolyCam. MapCam's objective was to take images of Bennu as a point-source during the approach, as well as to scan for outgassing plumes and potential satellites [29]. SamCam's objective was to continuously document the sampling site before, during and after the sample acquisition [29]. An image taken by SamCam documenting the Touch-And-Go (TAG) sampling manouvre can be seen in Figure 8. Finally, PolyCam's objective was to take detailed, high-resolution images of the sample site to study Bennu's surface texture and morphology [29]. This made the PolyCam images the most relevant ones for my thesis, as I wanted to look at high resolution images in order to study boulder morphology. Therefore, the images studied in this thesis are all taken by PolyCam.

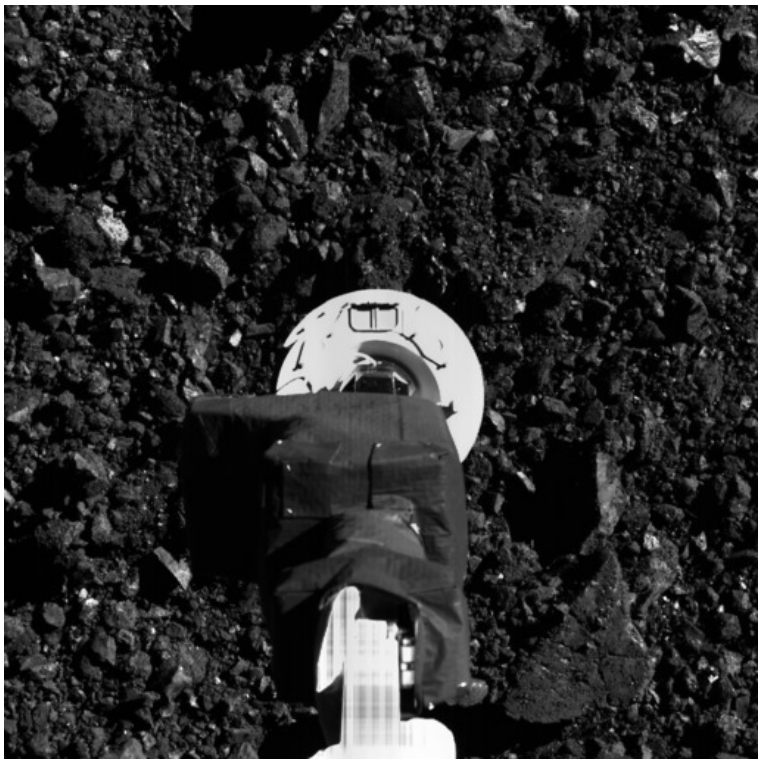

Figure 8: A SamCam image of the TAG manoeuvre [30].

When OSIRIS-REx arrived at Bennu, its surface was a lot more rugged and contained more larger boulders than expected. It also did not contain as many areas of centimeter to millimeter scale regolith as expected, which is what was needed for its Touch-And-Go Sample Acquisition Mechanism (TAGSAM) to be able to acquire its sample of at least 60 grams [18]. Figure 9 shows the phases of the mission. This made landing more difficult, but four potential landing sites were identified. They were named Nightingale, Kingfisher, Osprey and Sandpiper, and in the end, Nightingale was chosen as the sample site [18]. The four candidate sample sites can be seen in Figure 10. The sample was successfully collected from the Nightingale site on the 20th of October 2020 [18].

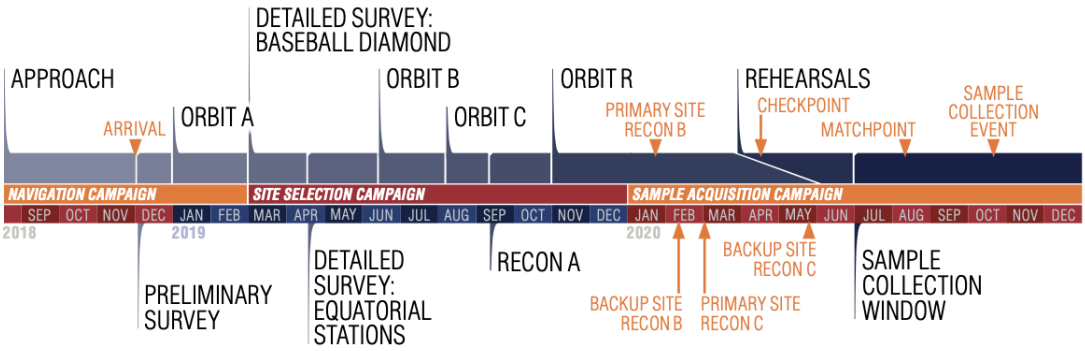

Figure 9: The mission phases of OSIRIS-REx [18]. The images in this paper are from the "Recon A" phase.

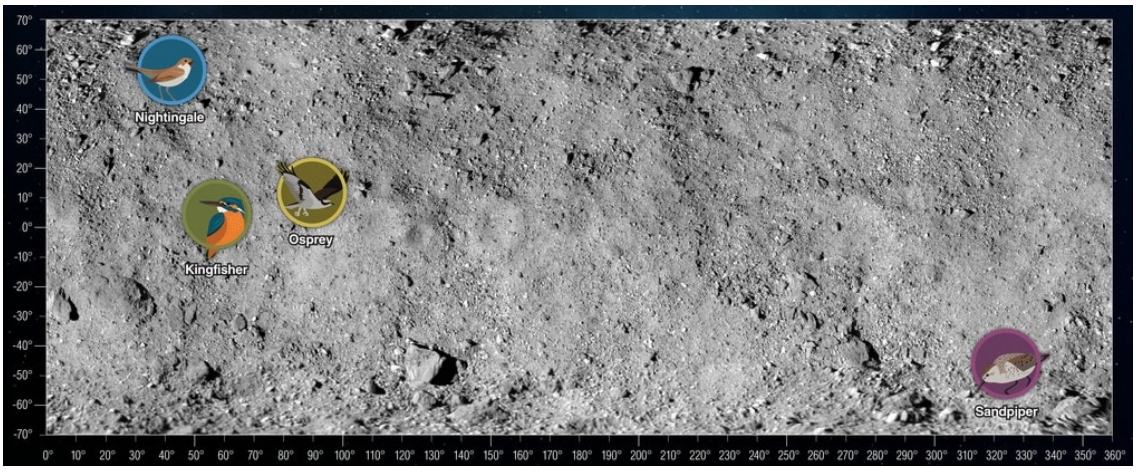

(a) The location of the four candidate sample sites. Image from [32].

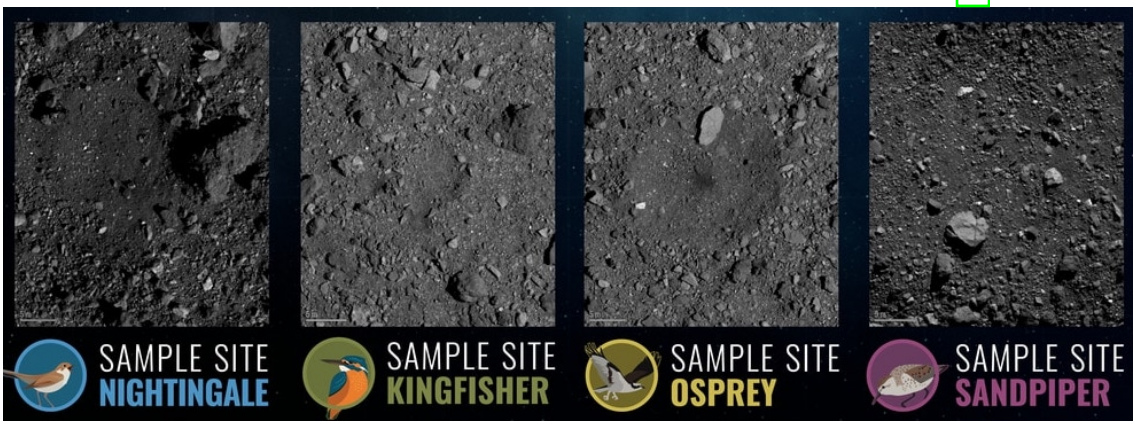

(b) Close up of the four candidate sample sites. Image from [32].

Figure 10: The four candidate sample sites of OSIRIS-REx: Nightingale, Kingfisher, Osprey and Sandpiper [32].

The sample was returned to Earth in September 2023, and it contained 120 grams of material, so twice as much as the original goal [28]. Preliminary analysis of the returned sample revealed that Bennu contains phyllosilicates, carbonates, magnetite, and pyrrhotite, which indicate that the asteroid has experienced aqueous alteration in the past [8]. Further analysis of the sample is underway.

3 Theory

In order to study boulder morphology, shape factors - sometimes also called morphologic descriptors - are used. These are scale independent parameters that can give information about a boulder's roughness and compactness. I chose to investigate two shape factors that describe boulder roughness, and two that describe how compact a boulder is.

For boulder roughness, I studied circularity (C) and solidity (S). Equation 3 show the equation for circularity [4]. A is the area of the boulder and P is the perimeter of the boulder, which can be seen in Figure 11. Circularity shows how smooth a boulder outline is, i.e. the extent to which its boundary resembles that of a circle. It does this by dividing the boulder area by the area of a circle that has a circumference equal to the boulder perimeter. This means that a circle has a circularity of 1, while a boulder with rough and uneven edges has a lower circularity, as the perimeter of a rough boulder is larger than the circumference of a circle with the same area as the boulder. This parameter is also sometimes referred to as perimeter sphericity.

In order to find the area of a circle with the same circumference as that of the boulder's perimeter, I first needed to find the radius of that circle, r_1, as seen in Equation 1.

$$P = 2\pi r_1 \Rightarrow r_1 = \frac{P}{2\pi} \tag{1}$$

I could then find the area of the circle, A_1, by inserting Equation 1 into the equation of a circle's area, as seen in Equation 2.

$$A_1 = \pi r_1^2 = \pi(\frac{P}{2\pi})^2 = \frac{P^2}{4\pi} \tag{2}$$

I then divided the area of the boulder with the area of the circle to find the circularity, as seen in Equation 3.

$$C = \frac{A}{A_1} = \frac{A}{\frac{P^2}{4\pi}} = \frac{4\pi A}{P^2} \tag{3}$$

Equation 4 shows the equation for solidity [4]. H is the area of the convex hull of the boulder, which can be seen in Figure 11. Solidity shows the extent of concavity or convexity

of a boulder by dividing the boulder's area with the area of its convex hull. This means that a boulder without any uneven or rough edges (a convex boulder) has a solidity of 1, as the convex hull has the same shape as the boulder. A rough boulder has a low solidity value, as the convex hull has a larger area than the boulder.

$$S = \frac{A}{H} \tag{4}$$

To study the compactness of the boulders, I looked at the shape factors elongation (E) and roundness (R). Equation 5 shows the equation for elongation [4]. a is the major axis of the boulder and b is the minor axis of the boulder, as seen in Figure 11. Elongation shows how elongated a polygon is by dividing its minor axis with its major axis. A compact boulder has an elongation of 1 as its two axes are the same size, while a highly elongated boulder has a small elongation as its major axis is larger than its minor axis. Note that a square also has an elongation of 1, so elongation is not necessarily related to the sphericity of a boulder but rather its compactness[1].

$$E = \frac{b}{a} \tag{5}$$

Equation 7 shows the equation for roundness [4]. Roundness describes how close a boulder's shape is to a circle by dividing the area of the boulder with the area of the minimum circumscribed circle surrounding it. The minimum circumscribed circle of a boulder is illustrated in Figure 11. A boulder with a high roundness value has a minimum circumscribed circle with an area close to that of the boulder, so it would have a roundness close to 1. An elongated boulder has a much smaller area than that of its circumscribed circle, resulting in a low roundness value. This parameter is also sometimes called area sphericity.

The minimum circumscribed circle has a diameter the same length as the boulder's major axis, a. Its area, A_2 can then be described with Equation 6:

$$A_2 = \pi(\frac{a}{2})^2 = \frac{\pi a^2}{4} \tag{6}$$

Then, the area of the boulder can be divided with the area of the circumscribed circle to find

[1]Note that the term compactness is sometimes also used for the square root of the above defined circularity. In this thesis, when using the term compactness, I collectively refer to the parameters solidity and roundness.

roundness, as shown in Equation 7.

$$R = \frac{A}{A_2} = \frac{A}{\frac{\pi a^2}{4}} = \frac{4A}{\pi a^2} \tag{7}$$

Figure 11 illustrates the parameters needed to calculate the four shape factors mentioned above. A circle with the same area as the boulder (not sketched for illustrative purposes) would be a circle with the same area A as the blue region in the image.

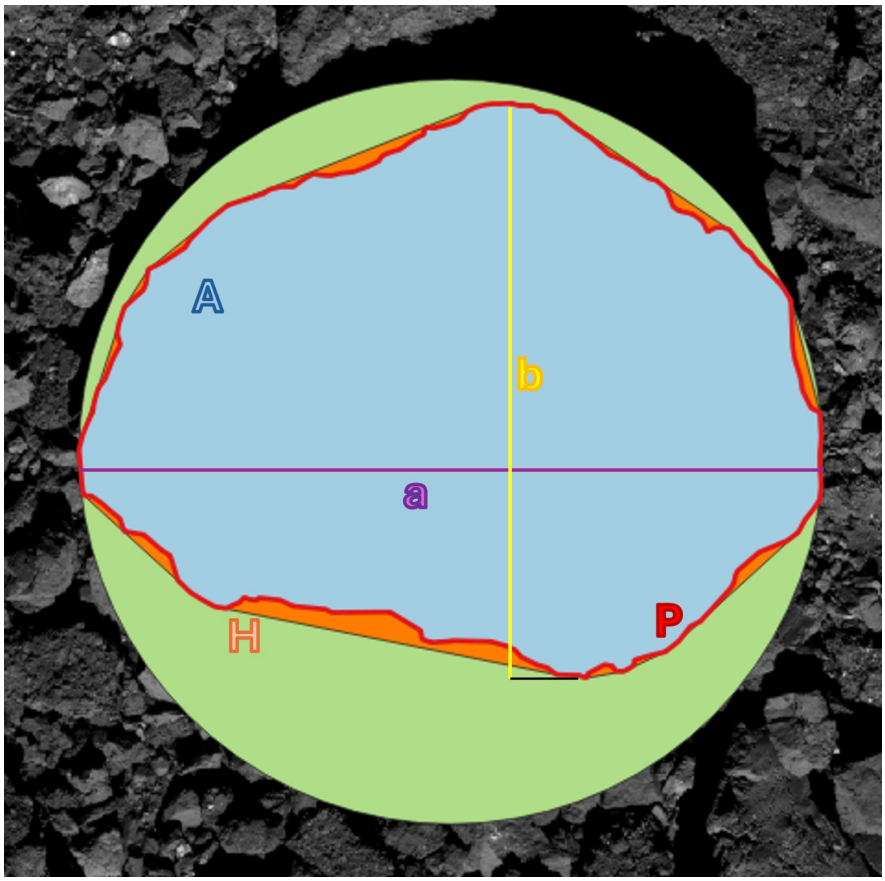

Figure 11: The parameters needed to calculate the shape factors used in this thesis. The blue region is the area A of the boulder, the red line is the perimeter P of the boulder, the purple and yellow lines illustrate the major a and minor b axes of the boulder, the orange region is the convex hull area H, and the green circle is the minimum circumscribed circle.

4 Methodology

The images I studied were taken by the OSIRIS-REx Camera Suite (OCAMS) onboard the OSIRIS-REx spacecraft, and retrieved from the mission database, found in NASA's Planetary Data System [29]. The identification and mapping of boulders was done with the open-source software Quantum Geographic Information System (QGIS) [27]. I uploaded the chosen images to QGIS one by one and traced over the boulders I observed in order to create a shapefile with the shapes of the boulders. This work derives a two dimensional representation of a three dimensional boulder. Thus, the observation angle (e.g. emission angle of the images) of the boulders' morphology should be statistically independent of the observation direction. For consistency with other works [4, 23], I decided to map boulders on non-projected images. As shape factors are not size dependent, they can still be analyzed without determining the true size of the boulders. The images also have a relatively small field of view (less than 15 m), and these factors contributed to my decision to use non-projected images.

If a boulder was smaller than 15 pixels across its shortest axis, I determined that it was too small to be included. This is because such small boulders are pixelated, so it is difficult to see the exact outline of the boulder. For consistency in mapping resolution, I maintained a constant zoom in each of the images, making the boulders four times larger than in the original image. This was done by using QGIS's built in zoom using the mouse wheel, each zoom of the wheel makes the image twice as large. They were also all plotted on the same monitor, so the display was the same for each image. When mapping the boulders, I decided the outline based on the visible edges of the boulders. The outline could be seen both with the help of shadows around it, and the texture difference between the boulder and the regolith it laid on. I used roughly one point in the polygon every 3 to 6 pixels.

After the mapping was completed, I started performing the calculations. The parameters I needed in order to calculate the boulders' shape factors mentioned in section 3 were: area A, perimeter P, major axis a, minor axis b and convex hull area H of the boulder. I was able to use pre-programmed routines in QGIS to find the necessary parameters. I found A and P by using the QGIS function "add geometry information", which shows the area and perimeter of all created polygons. I then used minimum oriented bounding boxes to find a and b, as seen in Figure 12a. The orientation of the boxes also gave me the information about the orientation of the boulders (β). The convex hull area could be found by using QGIS's convex

hull tool, as seen in Figure 12b. After I had added these shapes, I exported the data to the commercial spreadsheet software Microsoft Excel in order to perform the calculations.

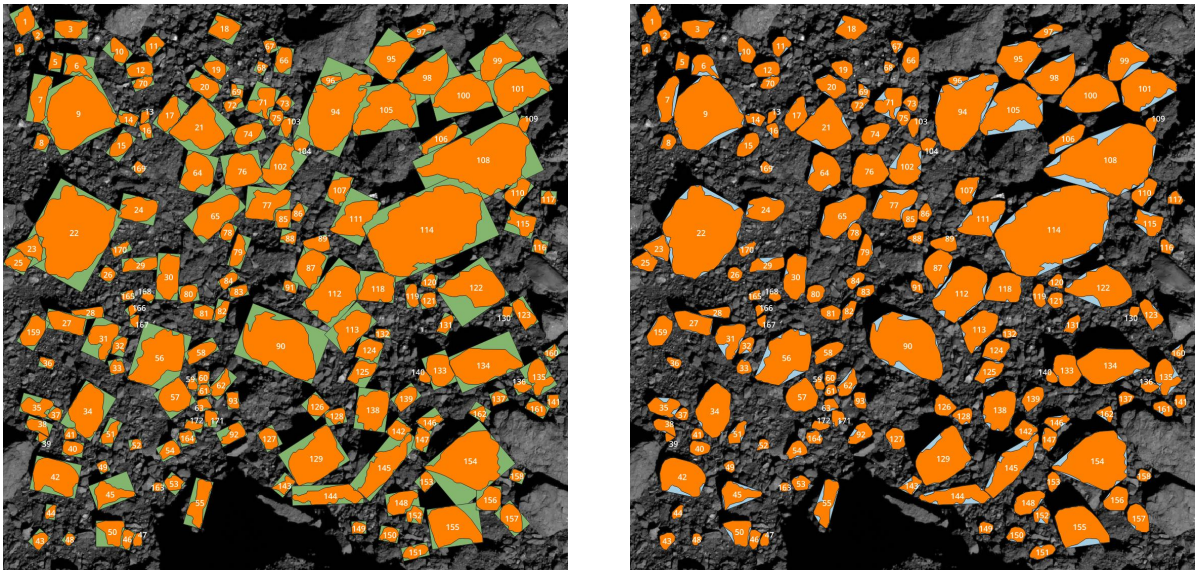

(a) The green boxes are the bounding boxes. The orange polygons are the mapped boulders. The numbers refer to individual boulders, and were used for tracking purposes only.

(b) The blue shapes are the convex hulls. The orange polygons are the mapped boulders. The numbers refer to individual boulders, and were used for tracking purposes only.

Figure 12: Example of the mapped boulders (orange) and the geometric features added in QGIS (Image ID: 20191026T213742S732_pol_iofL2pan).

Adding these geometric shapes in QGIS allowed me to find area A, perimeter P, major axis a, minor axis b and convex hull area H of the boulders. All the parameters from QGIS were in pixels, so I also had to convert them to meters. This is not necessary for shape factors since they are size independent, but I also wanted to assess boulder sizes, so I needed to measure the boulder axes. This was also done in Excel by multiplying the number of pixels with the resolution for the image. The pixel resolution was provided with the images' meta data. I then calculated the shape factors mentioned in section 3 in Excel. Finally, after I generated the data, I exported it to MathWorks's proprietary software Matlab for further analysis and plotting.

4.1 Data Selection

As mentioned in subsection 2.3, I chose to only study images taken by PolyCam because of their high resolution. I wanted to use high resolution images to look at comparatively small scale regolith pieces and make use of this high resolution dataset that is currently unmatched by any other asteroid mission. I studied three regions within the Smooth Unit, and three regions within the Rugged Unit, as identified by Jawin et al. (2022) [14]. Within each of the six regions, I looked at 5 separate images that did not overlap so no boulder would be mapped twice, leading to a total of 30 images. To maintain a good pixel resolution, I decided on 0.015 meter per pixel as the maximum resolution. By using the image browser on NASA's web-page Planetary Data System (PDS) Small Bodies Node[2] [34], I viewed which mission phases had the best resolution and covered the most areas. I found that the Reconnaissance A phase of the mission provided the largest number of regions with a good enough resolution. In the Reconnaissance A phase, the spacecraft was at an altitude of 1000 to 1250 meters [18].

I then selected all images taken by PolyCam during the Reconnaissance A phase that had a better resolution than 0.015 m/pixel. This allowed me to see which regions of Bennu had satisfactory resolution. I overlaid these regions with the map created by Jawin et al. (2022) [14]. This allowed me to identify three regions in the Smooth and Rugged Units to study in good resolution. Figure 13 shows these chosen regions. However, since I focused on high resolution images, larger boulders tend to be excluded. All images have a pixel size of 1024 × 1024, and Equation 8 show that an image with a resolution of 0.015 meters per pixel would then be only approximately 15 meters across.

$$1024 \cdot 0.015 \text{ m} = 15.36 \text{ m} \tag{8}$$

This means that boulders larger than 15 meters exceed the image dimensions. Because I only mapped boulders that fit entirely within the image, only boulders smaller than 15 meters were mapped. Considering that 0.015 meters per pixel was the lowest resolution I used, several of the images used in this work have better resolution, so that the largest identifiable boulders on these images are even smaller.

[2]Webpage: https://sbib.psi.edu/data/PDS-Bennu/index.html

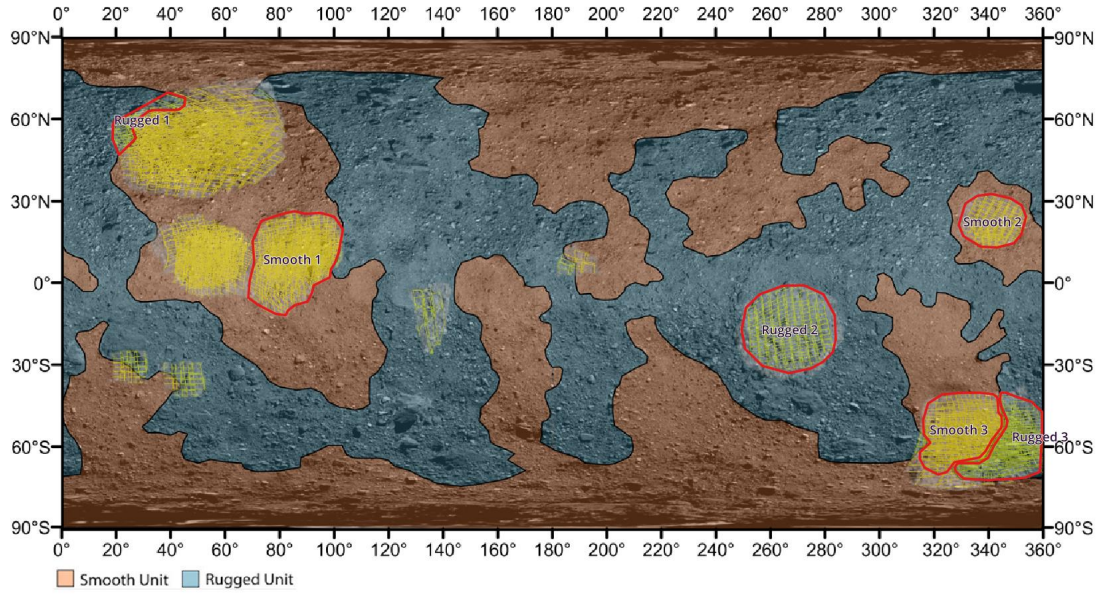

Figure 13: Bennu's two geological units as identified by Jawin et al. (2022) [14] overlaid with the regions with a resolution better than 0.015 meter per pixel. The yellow patterns represent images taken with a resolution better than 0.015 meter per pixel. The red, circled areas show the six regions chosen for study.

When I had decided on the regions for study, I chose the five images with the best resolution that did not overlap in each of the six regions. Figure 13 shows the placement of the 30 chosen images as viewed in the image browser in the PDS Small Bodies Node [34]. Table 2 lists the chosen images. The resolutions, solar incidence angles, emission angles, longitudes and latitudes were taken from the available information in the mission data base [30], and the image area was approximated by multiplying the image size in pixels with its resolution. The solar incidence angle is the angle between the rays of the Sun and the normal of the surface in the image, and the emission angle is the angle between the spacecraft and the normal of the surface in the image. In the mission data base [30], the emission and solar incidence angles for each image are assuming a flat, idealised surface based on an underlying low resolution shape model of Bennu, even though in reality, the emission and solar incidence angles depend on the local topography of the surface.

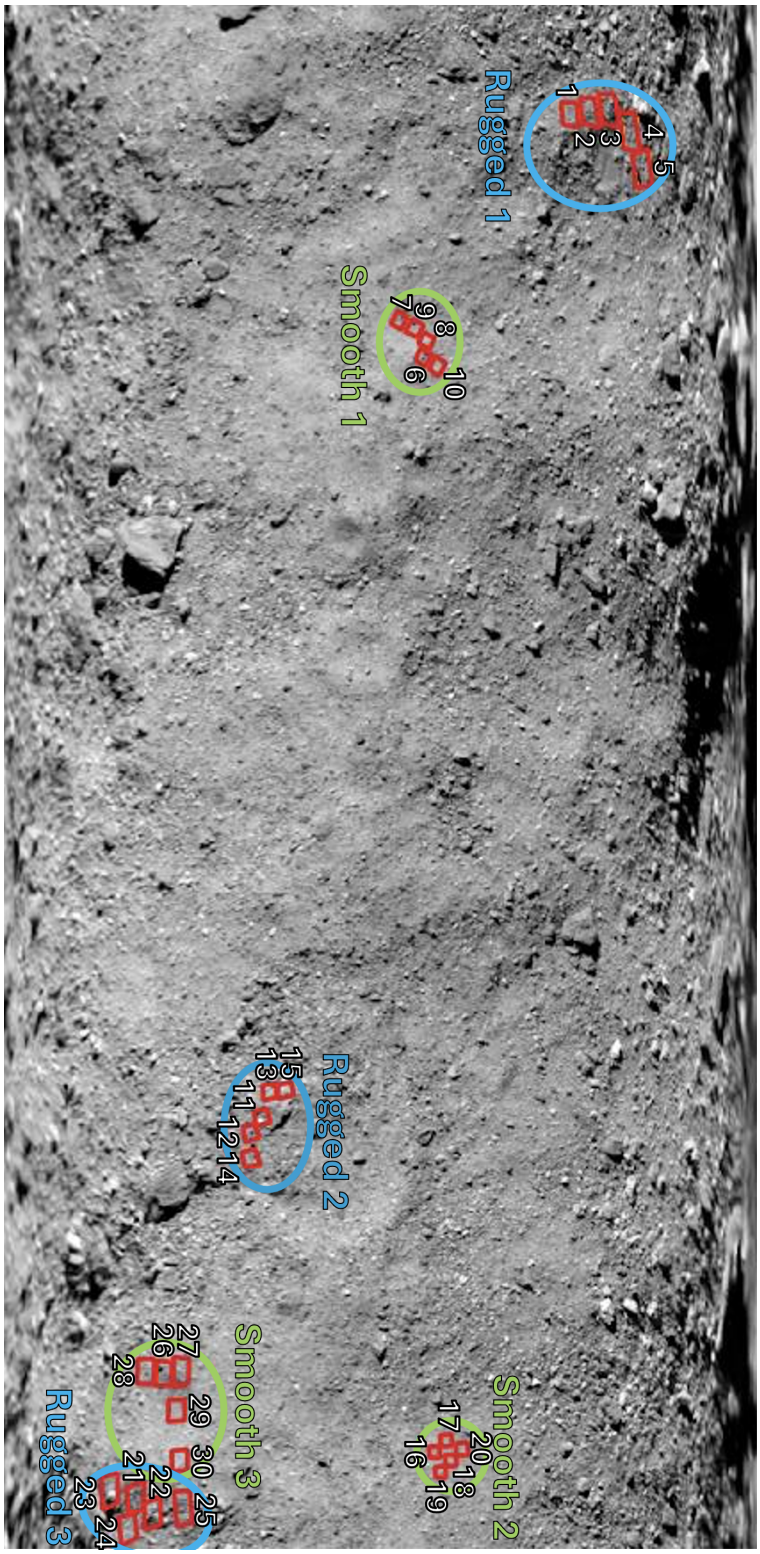

Figure 14: The 30 chosen images as viewed in the PDS Small Bodies Node (red squares). The Image IDs corresponding to the numbered images can be found in Table 2. The blue outlines represent the rugged regions and the green outlines represent the smooth regions. The image is flipped 90° for legibility.

Table 2: Parameters of the images used in this work.

Image ID (end with _pol_iofL2pan)	**Region**	**ID in Fig.14**	**Resolution (m/pxl)**	**Incidence angle (°)**	**Emission angle (°)**	**Lat.** (°)	**Long.** (°)	**Image area (m^2)**
20191026T220330S729	Rugged 1	1	0.0123	63.4	39.9	47.7	29.6	159
20191026T220320S574	Rugged 1	2	0.0124	65.9	43.0	51.9	28.7	161
20191026T220308S430	Rugged 1	3	0.0125	68.6	46.7	56.3	28.1	164
20191026T220212S730	Rugged 1	4	0.0127	73.2	52.1	61.5	33.6	169
20191026T213742S732	Rugged 1	5	0.0133	70.1	45.1	64.1	42.0	185
20191012T222715S982	Smooth 1	6	0.0123	43.1	37.0	14.4	84.7	159
20191012T223340S501	Smooth 1	7	0.0123	42.7	41.3	8.8	76.6	159
20191012T223103S875	Smooth 1	8	0.0123	45.1	36.8	15.1	81.1	159
20191012T223409S486	Smooth 1	9	0.0124	45.8	39.8	12.2	78.3	161
20191012T222650S984	Smooth 1	10	0.0124	45.6	35.9	17.5	86.9	161
20191005T202551S161	Rugged 2	11	0.0135	25.8	20.5	-22.3	258.0	191
20191005T202438S908	Rugged 2	12	0.0134	28.7	17.1	-24.9	261.5	188
20191005T202949S197	Rugged 2	13	0.0135	23.9	23.4	-20.6	252.2	191
20191005T202016S711	Rugged 2	14	0.0135	28.6	16.6	-24.9	267.4	191
20191005T203012S510	Rugged 2	15	0.0135	20.2	28.1	-17.3	251.9	191
20191026T223125S701	Smooth 2	16	0.0107	28.0	1.1	16.9	334.3	120
20191026T223241S428	Smooth 2	17	0.0107	29.8	3.7	19.5	331.6	120
20191026T222923S826	Smooth 2	18	0.0108	31.1	4.1	20.6	336.2	122
20191026T222806S995	Smooth 2	19	0.0108	29.3	0.6	18.2	338.7	122
20191026T223039S912	Smooth 2	20	0.0108	33.0	8.3	23.1	333.6	122
20191005T193228S655	Rugged 3	21	0.0143	58.3	32.6	-51.1	344.9	214
20191005T193048S900	Rugged 3	22	0.0143	55.1	31.0	-47.3	348.1	214
20191005T193407S925	Rugged 3	23	0.0144	63.2	36.6	-56.8	342.5	217
20191005T193034S211	Rugged 3	24	0.0144	60.6	36.6	-52.8	351.5	217
20191005T194948S256	Rugged 3	25	0.0145	57.6	42.4	-40.4	346.7	220
20191005T194314S115	Smooth 3	26	0.0140	50.5	17.0	-44.7	316.4	206
20191005T200500S273	Smooth 3	27	0.0140	52.1	29.4	-40.8	315.6	206
20191005T194336S525	Smooth 3	28	0.0140	54.4	21.3	-48.8	315.9	206
20191005T193926S463	Smooth 3	29	0.0140	47.9	16.8	-41.8	324.8	206
20191005T193458S053	Smooth 3	30	0.0140	47.9	21.4	-41.1	336.1	206

5 Data Assessment and Validation

5.1 Certainty levels

During the mapping, the shapes of the boulders were sometimes challenging to determine. Shadows and regolith may have covered parts of boulders, so the exact outline of the boulder was not visible. An example of a boulder partly covered by shadows can be seen in Figure 15a, and one partly covered by regolith can be seen in Figure 15b. As can be seen, it is challenging to determine where the actual boundary of the boulder is. It can also be difficult to determine if a crack in the boulder has completely separated it to two different boulders or if it is superficial. Figure 15c shows a boulder that has a crack running through it. It is challenging to tell if the crack has completely split the boulder into two parts, or if it is an intact boulder with a crack. It can also be difficult to determine if shapes close to each other are part of the same boulder or several boulders laying close to each other. An example of this can be seen in Figure 15d. Because of this, I assigned a certainty level to each of the mapped boulders, shown in Table 3. That meant that I could draw the boulders' boundaries to the best of my ability, and then I could assign a certainty level depending on how sure I was of the outline I had drawn.

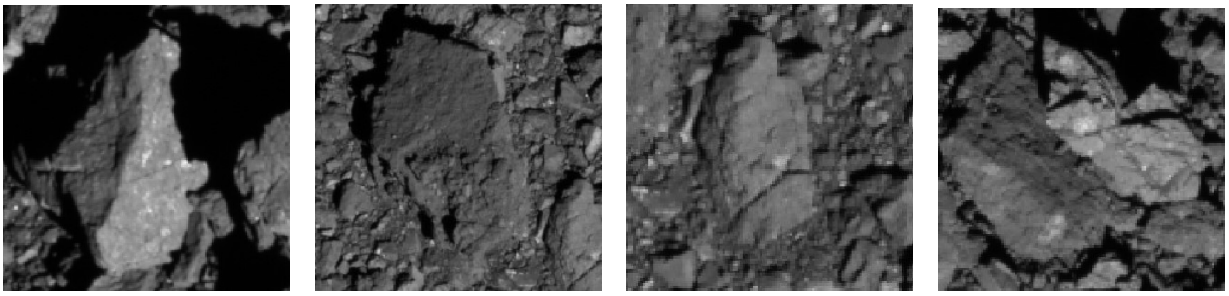

(a) Boulder partly hidden by shadow.

(b) Boulder covered by regolith.

(c) Boulder with a crack.

(d) Boulders with unclear outline.

Figure 15: Examples of different features that can make mapping a clear boulder outline difficult.

Table 3: Grades for certainty levels of boulder outline

Certainty level	Grade
Very certain of outline	1
Outline potentially partially covered	2
Outline significantly covered	3

Figure 16a shows an example of a boulder assigned certainty level 1. The outline of the boulder can be seen clearly, and is not covered by shadows or regolith. Figure 16b shows an example of a boulder assigned certainty level 2. Most of the outline is fairly clear, but one section is partly covered by the shadow of another boulder. This means that the outline may be a slightly off. Figure 16c shows an example of a boulder assigned certainty level 3. Here, it is clear that the top part of the boulder is significantly covered by the shadow of another boulder, while the bottom part is covered by small regolith particles. This means that the visible outline is uncertain, which is why it has level 3.

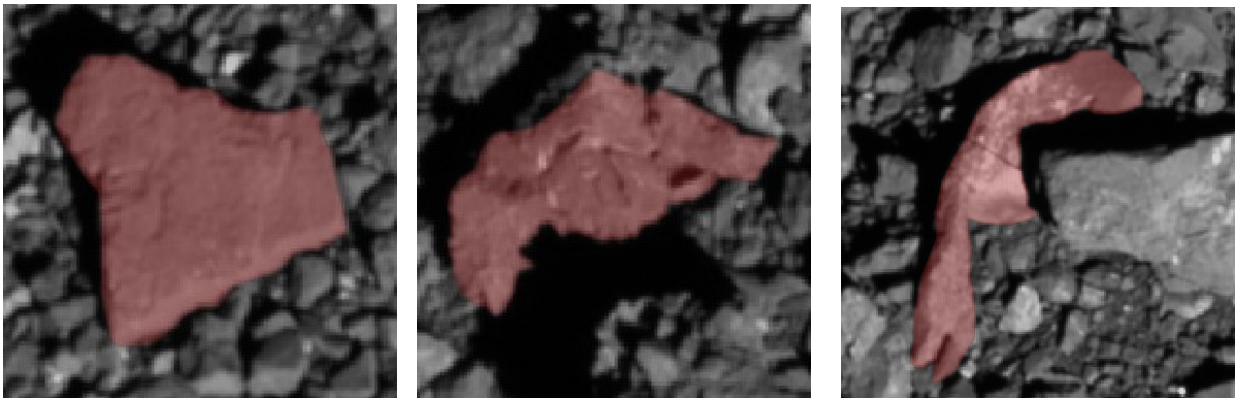

(a) Example of certainty level 1. (b) Example of certainty level 2. (c) Example of certainty level 3.

Figure 16: Example of the different certainty levels. The red shaded area illustrates the mapped boulder.

5.2 Effect of shadows

Subsequent to the assignment of certainty levels to the boulders, I decided to exclude boulders with certainty level 3 to avoid the possible misinterpretations of their morphology to influence my results. In the next step I examined if level 2 was appropriate to use. The main issue with these kind of uncertain boulders is that they are partly covered by shadows. To assess

how shadows and the related solar incidence angle affect the shape and orientation of the boulders I mapped, I investigated the general orientation of the boulders. Since I wanted to know how the solar incidence angle affects the interpretation of the orientation of the boulders due to shadows hiding them, I decided to study the image that had the largest solar incidence angle in each region. However, because the images were non-projected, I could not directly compare the solar incidence angle with the boulder orientation angle, so instead I approximated the angle of the shadows (see α in Figure 17), which can be seen in Table 4. The angles of the boulder and shadow orientation are referenced in the image coordinates of each image. Histograms of the orientation angle can be seen in Figure 18a to Figure 20b. The orientation angle shown in the histograms refers to the angle of the oriented minimum bounding box that surrounds each boulder (see β in Figure 17) in the images. In other words, the angle shown is the angle of the boulder orientation in the non-projected image frame, not the real orientation angle of the boulder. This is why the orientation is compared to the angle of the shadows in the images, not to the solar incidence angle.

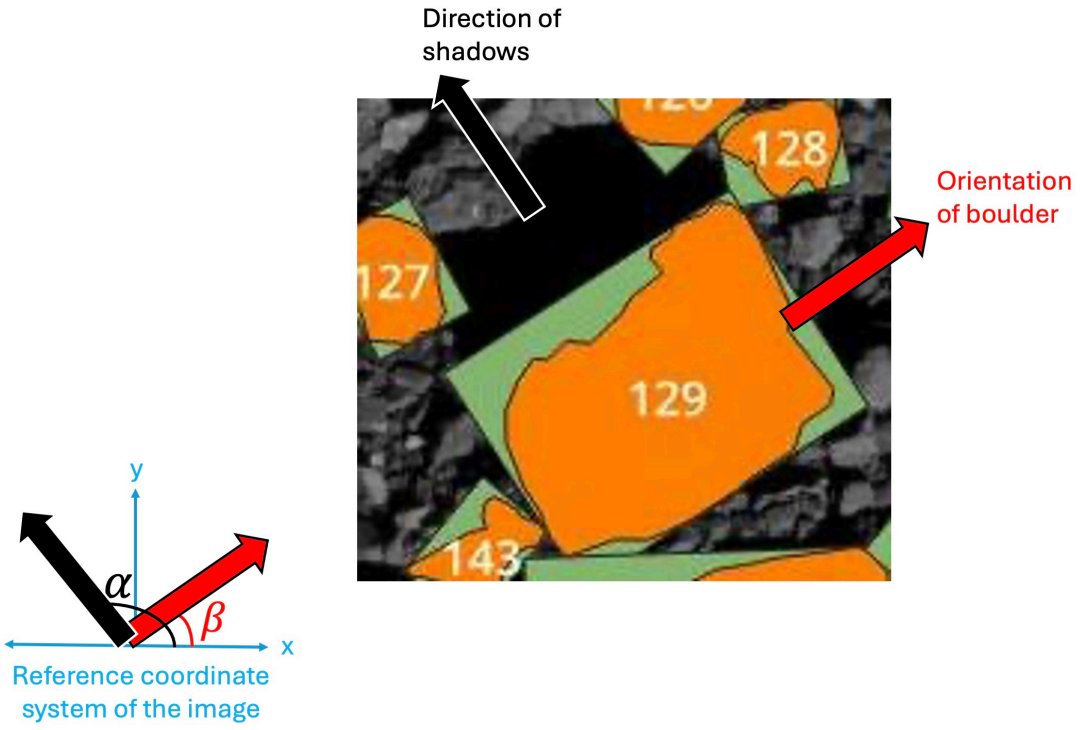

Figure 17: Illustration of α, the approximate angle of the shadows (black arrow), and β the orientation of the boulders (red arrow) in the image, with respect to image coordinates (blue axes). The orange polygons are the mapped boulders, the green boxes are the bounding boxes, and the numbers are a labelling system used only to keep track of each boulder.

Table 4: The images used to study possible effects of solar incidence and emission angles

Image ID	Region	Solar incidence angle	Angle of shadows	Emission angle
20191026T220212S730	Rugged 1	73.2	135	52.0
20191012T223409S486	Smooth 1	45.8	90	39.8
20191005T202438S908	Rugged 2	28.7	90	17.1
20191026T223039S912	Smooth 2	33.0	120	8.3
20191005T193407S925	Rugged 3	63.2	90	36.6
20191005T194336S525	Smooth 3	54.4	90	21.3

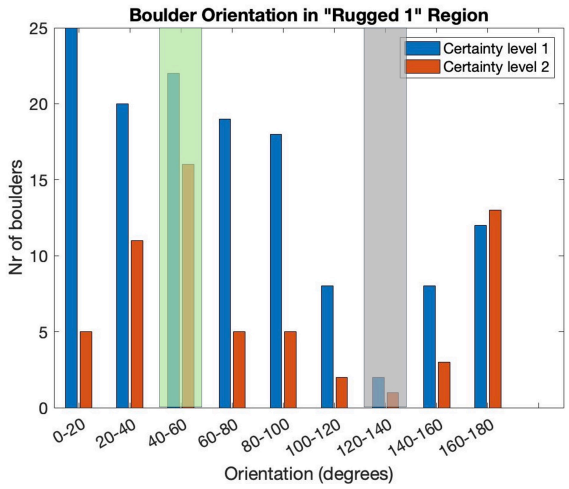

(a) Boulder orientation for an image in the Rugged 1 region. The shadow is angle 135°. Image ID: 20191026T220212S730.

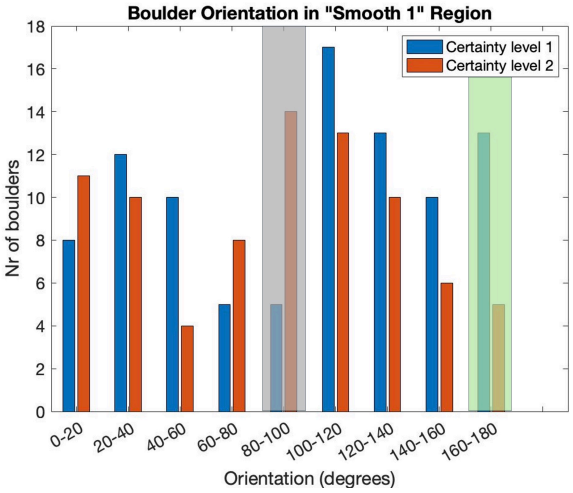

(b) Boulder orientation for an image in the Smooth 1 region. The shadow angle is 90°. Image ID: 20191012T223409S486.

Figure 18: Boulder orientation in the Rugged 1 and Smooth 1 regions. The grey shaded area is the bin containing the angle of the shadows, which is where I would expect to see the least boulders if an orientation bias is present. The green shaded area is the bin containing the angle perpendicular to the shadows, so where I would expect to see the most boulders if an orientation bias is present.

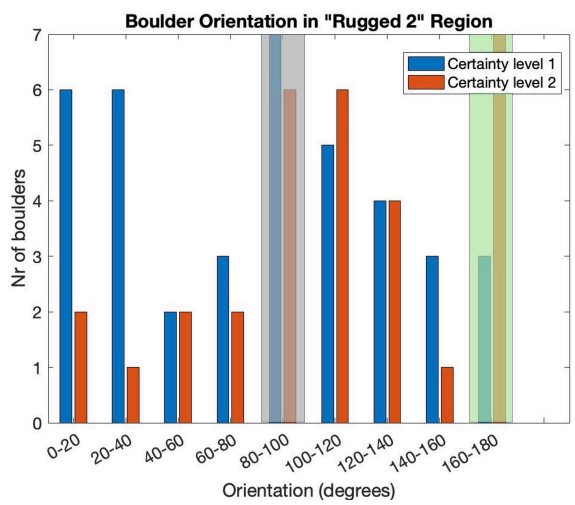

(a) Boulder orientation for an image in the Rugged 2 region. The shadow angle is 90°. Image ID: 20191005T202438S908.

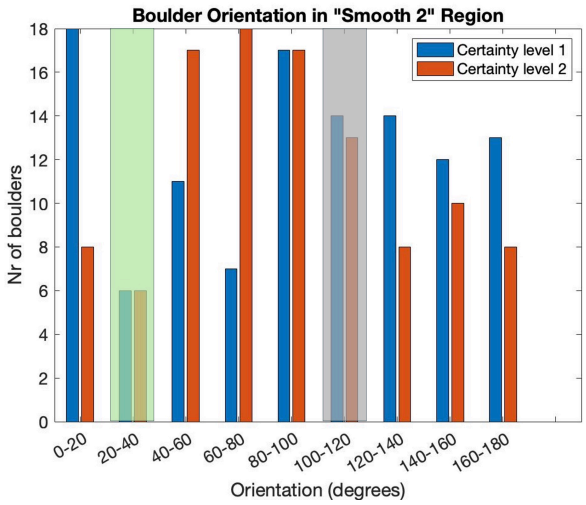

(b) Boulder orientation for an image in the Smooth 2 region. The shadow angle is 120°. Image ID: 20191005T193407S925.

Figure 19: Boulder orientation in the Rugged 2 and Smooth 2 regions. The grey shaded area is the bin containing the angle of the shadows, which is where I would expect to see the least boulders if an orientation bias is present. The green shaded area is the bin containing the angle perpendicular to the shadows, so where I would expect to see the most boulders if an orientation bias is present.

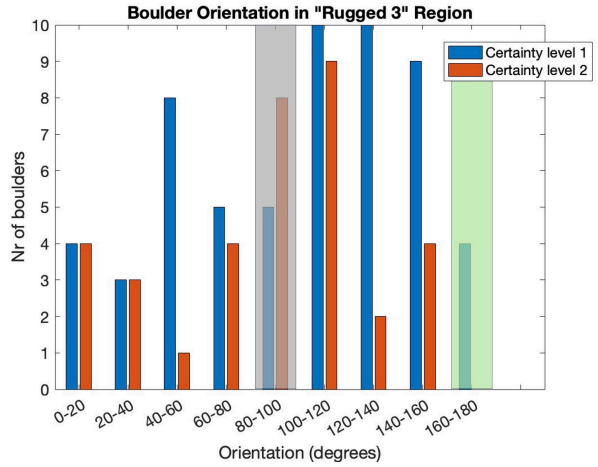

(a) Boulder orientation for an image in the Rugged 3 region. The shadow angle is 90°. Image ID: 20191005T193407S925.

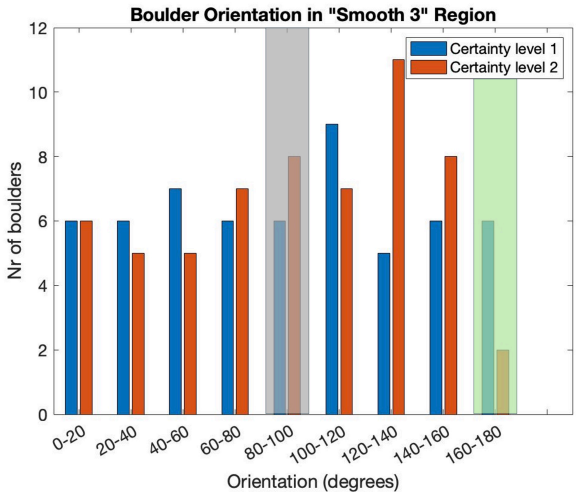

(b) Boulder orientation for an image in the Smooth 3 region. The shadow angle is 90°. Image ID: 20191005T194336S525.

Figure 20: Boulder orientation in the Rugged 3 and Smooth 3 regions. The grey shaded area is the bin containing the angle of the shadows, which is where I would expect to see the least boulders if an orientation bias is present. The green shaded area is the bin containing the angle perpendicular to the shadows, so where I would expect to see the most boulders if an orientation bias is present.

This was done to investigate whether or not the solar incidence angle, and thus the shadows would affect the derived orientation of the boulders by covering parts of them, creating an orientation bias. If it did affect it, I would expect to see a reduced number of boulders oriented in the same direction as that of the shadows, and the most boulders perpendicular to the shadows direction , i.e. a 90°shift. The shadows would preferentially cover the boulder from one side, which would make it appear longer in the direction perpendicular to the shadow direction. This is illustrated in Figure 21. Looking at Figure 18a, the least amount of boulders are indeed found in the bin containing the angle of the shadow, 135°. It can also be seen that for certainty level 2, it is the bin perpendicular to the shadows, 45°, that has the largest amount of boulders, but this is not the case for certainty level 1. This makes sense as the level 2 boulders were the ones that had unclear outlines partly due to shadows. Figure 19a has shadows at 90°, and in this figure we can also see that one bin perpendicular to it at 180°again contains the most amount of boulders for certainty level 2. However, for the rest of the images, there does not seem to be this trend of finding the most boulders

perpendicular to the shadows and the least in the same bin as the angle of the shadows. Indeed, Figure 19b even show the opposite, with the least amount of boulders in the bin containing the angle perpendicular to that of the shadows, 30°. Thus, since the overall trend seems to be that the shadows do not introduce an orientation bias in boulder orientation, I decided that it is acceptable to use both the boulders with certainty level 1 and level 2 for further analysis.

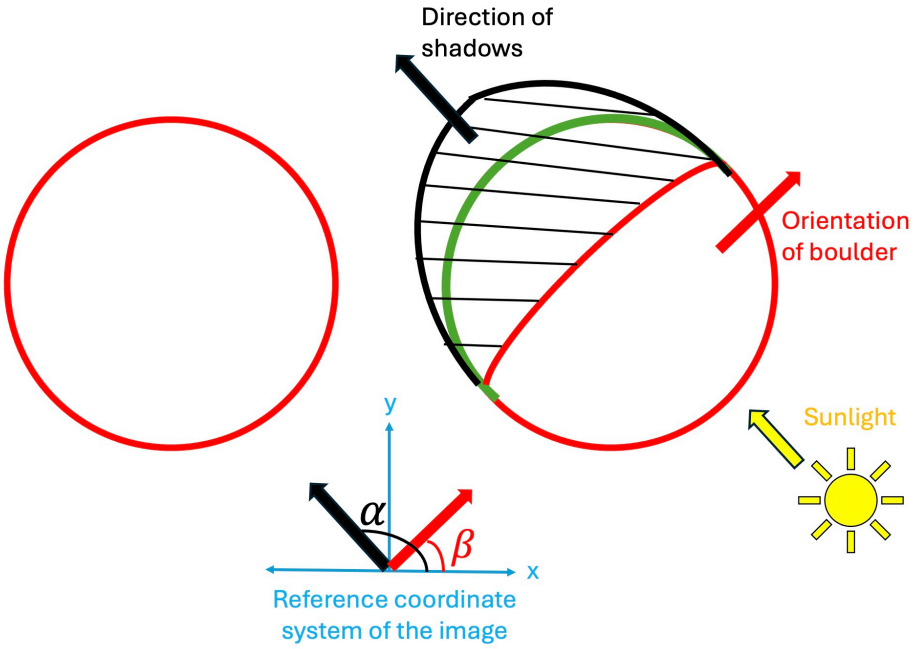

Figure 21: An illustration of the potential effect of shadows on the orientation of the boulder. On the left, there is a circular boulder (red circle) with no shadows, making it have an orientation of 0°. On the right, the same boulder is covered by shadows (black, lined area), and the new, red outline is missing part of the actual outline (green). The yellow arrow shows where the sun is coming from, and the black arrow shows the resulting direction of the shadows. The red arrow shows the orientation of the boulder (β), which is perpendicular to the direction of the shadows (α).

As can be seen in Figure 21, large shadows can also create an elongation bias. In order to check if images with larger incidence angles contained more elongated boulders (lower elongation value) as they contain more shadows, I plotted the incidence angles of the six images studied previously against the average elongation of those six images. The resulting plot can be seen in Figure 22. As can be seen in plot, a larger incidence angle does not lead

to significantly lower elongation values (more elongated boulders), which means that the possible elongation bias introduced by shadows is not large enough to invalidate my data.

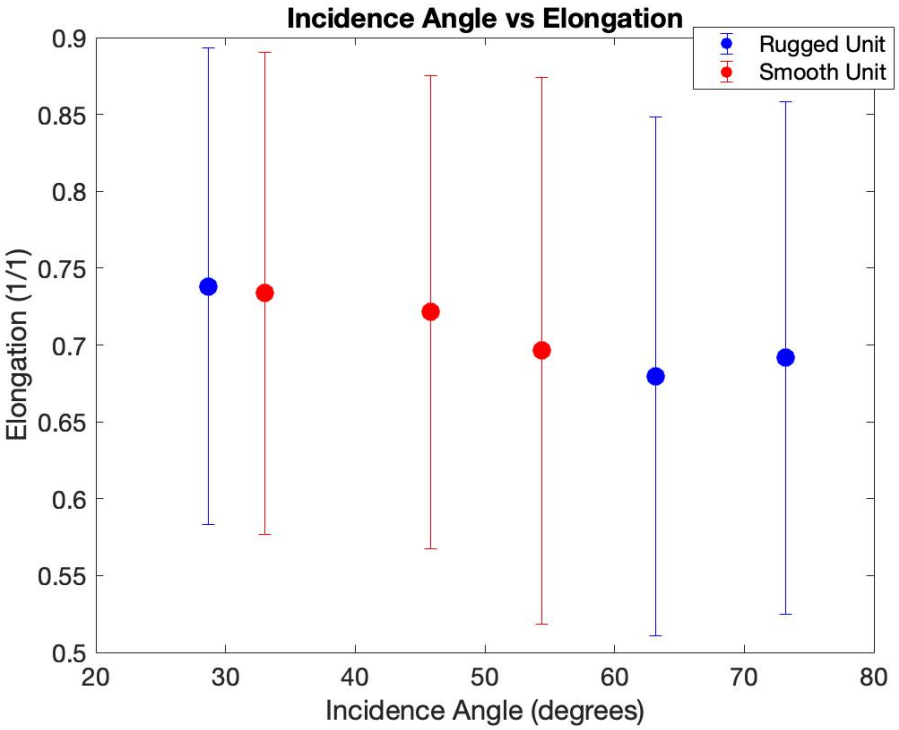

Figure 22: Average boulder elongation of all boulders in an analysed image against the incidence angle of that image.

5.3 Effect of emission angle

Another possible influence on the interpretation of the shape of the boulders is the emission angle. If the emission angle is large, this can create an elongation bias: if the spacecraft looks at a boulder from the side instead of from straight up, the shape may appear more stretched. In order to see if this may have an effect, I plotted the emission angle against elongation for the six images I used to study the effect of the solar incidence angle in the previous section (the values can be found in Table 4). The resulting graph can be seen in Figure 23.

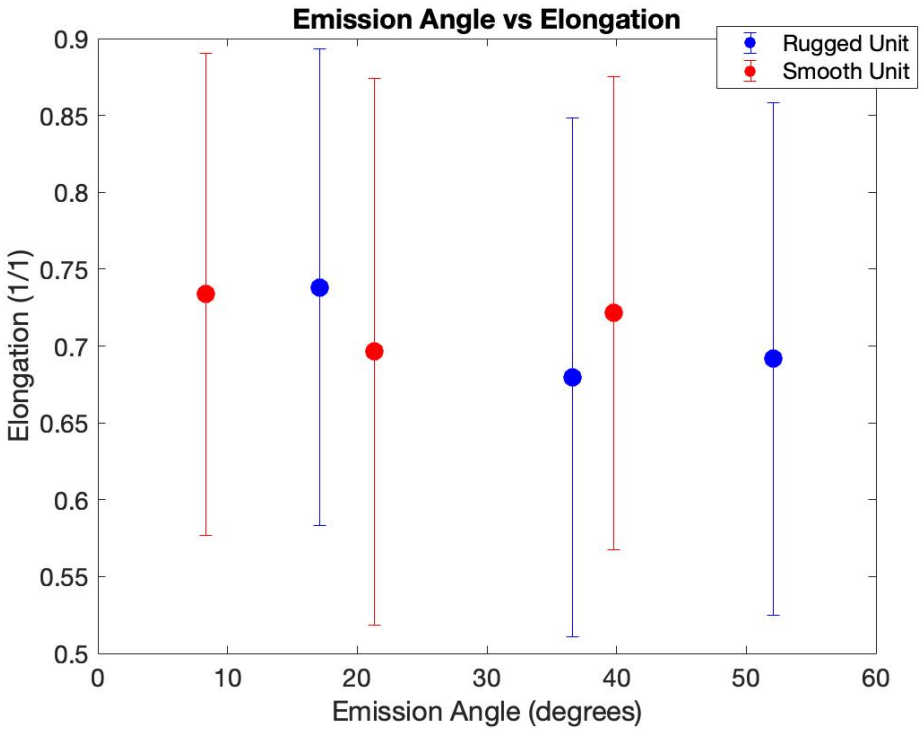

Figure 23: Boulder elongation of all boulders in an analysed image against the emission angle of that image.

If the emission angle created an elongation bias, I would expect to see more elongated boulders at higher emission angles. This means that the higher emission angles would have a lower elongation value (as higher elongation values means that the boulder is rounder). As can be seen in Figure 23, this does not seem to be the case. The elongation is fairly similar for all the emission angles, despite the large variation in emission angles. This indicates that the emission angle does not create a shape bias.

Following the validation analyses in this section, the following graphs in this report are therefore plotted using both certainty level 1 and 2. These analyses showed that, despite the varying illumination and imaging conditions of the images used in this work, the results are still comparable and a meaningful interpretation can be made.

6 Results

6.1 Maps

The resulting maps I created for each of the chosen regions can be seen here, three regions from the Rugged Unit and three regions from the Smooth Unit, with five maps each. The total number of boulders plotted in each region is shown in Table 5.

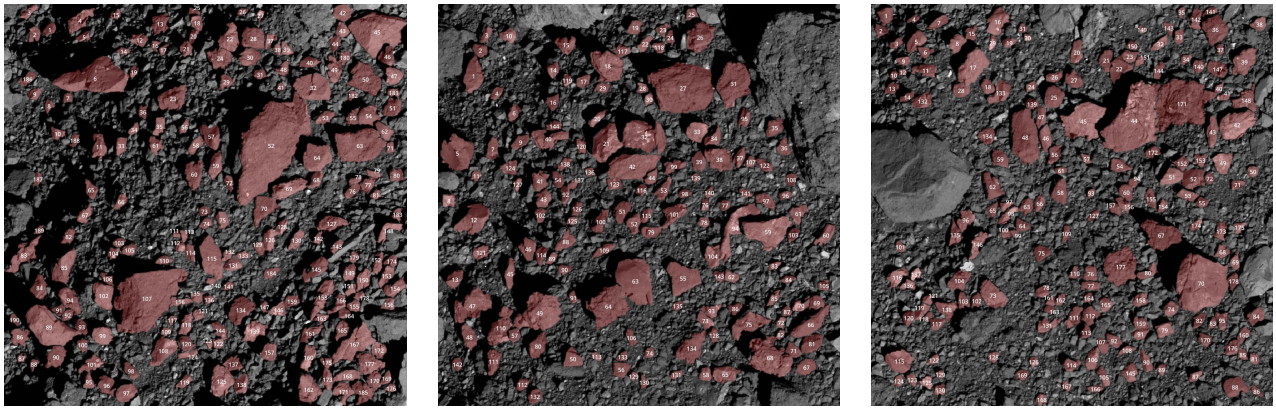

(a) **(b)** **(c)**

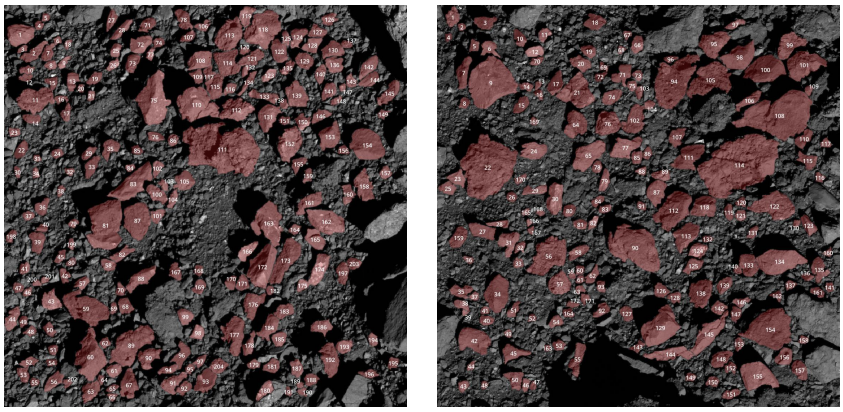

(d) **(e)**

Figure 24: The mapped boulders (red) from the Rugged 1 region. The numbers refer to individual boulder IDs that were assigned for tracking purposes only, image IDs: **(a)** 20191026T220308S430 **(b)** 20191026T220320S574 **(c)** 20191026T220330S729 **(d)** 20191026T220212S730 **(e)** 20191026T213742S732

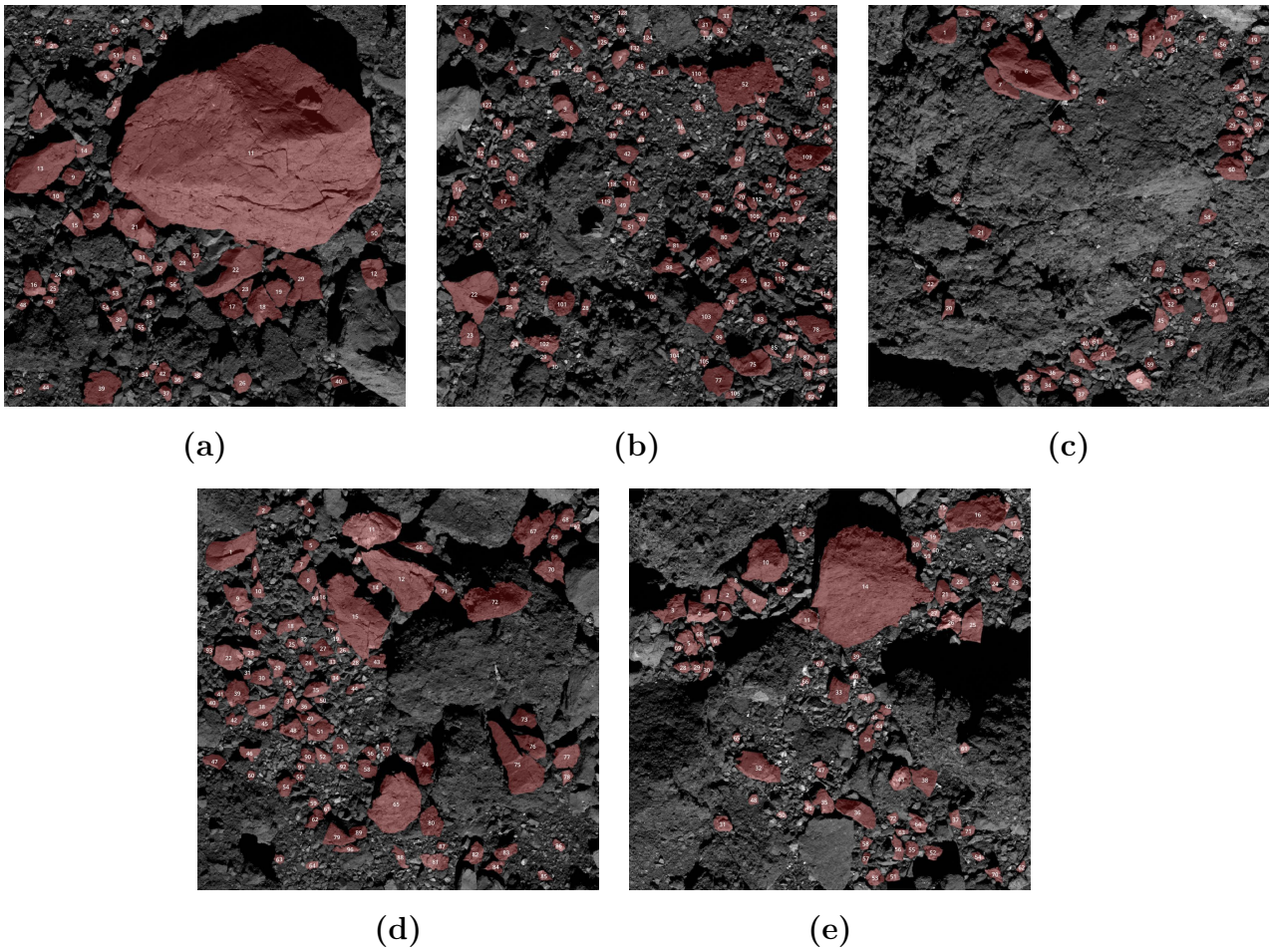

(a) **(b)** **(c)**

(d) **(e)**

Figure 25: The mapped boulders (red) from the Rugged 2 region. The numbers refer to individual boulder IDs that were assigned for tracking purposes only, image IDs: **(a)** 20191005T202551S161 **(b)** 20191005T202949S197 **(c)** 20191005T203012S510 **(d)** 20191005T202016S711 **(e)** 20191005T202438S908

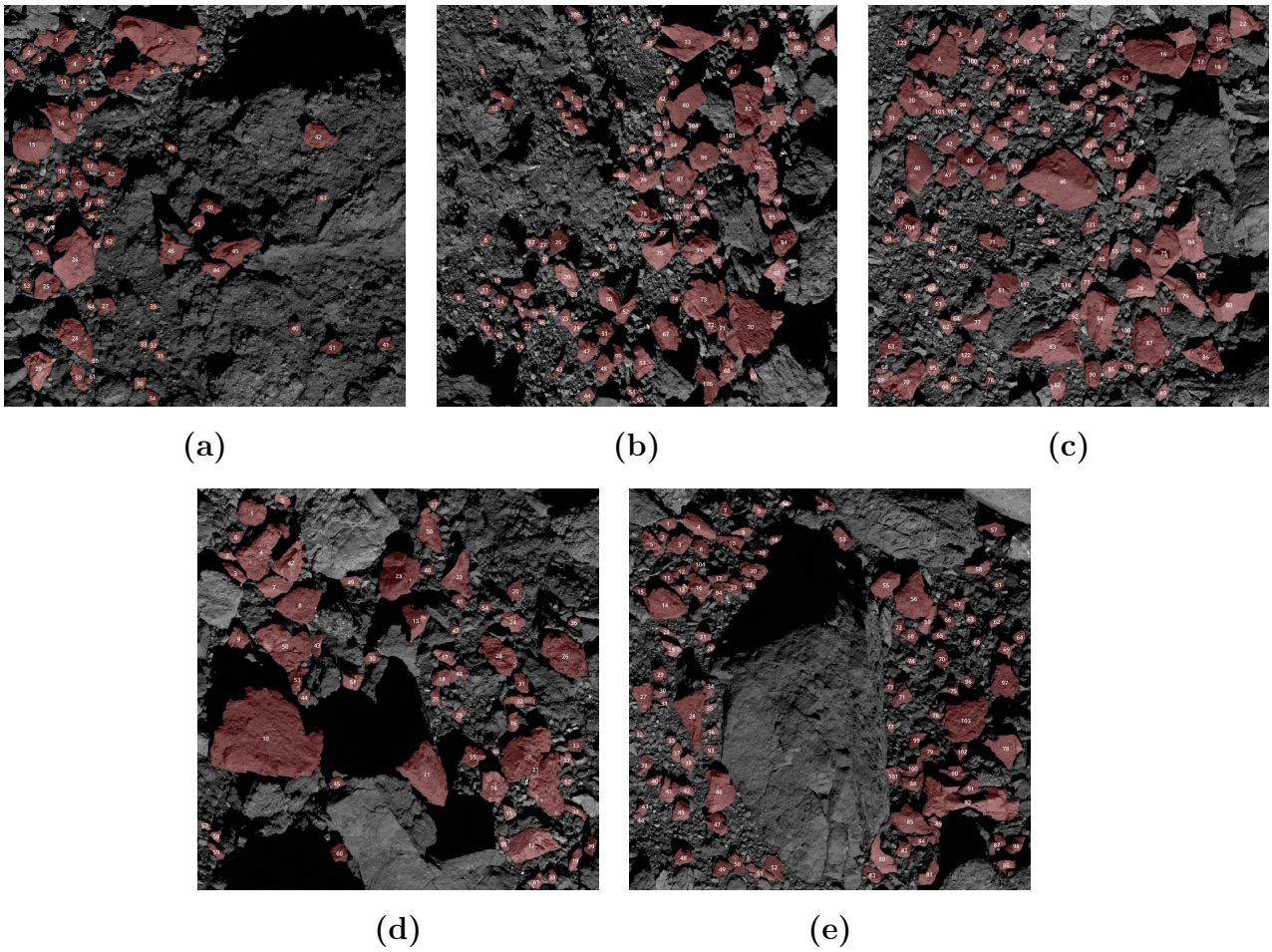

Figure 26: The mapped boulders (red) from the Rugged 3 region. The numbers refer to individual boulder IDs that were assigned for tracking purposes only, image IDs:: **(a)** 20191005T193034S211 **(b)** 20191005T194948S256 **(c)** 20191005T193228S655 **(d)** 20191005T193048S900 **(e)** 20191005T193407S925

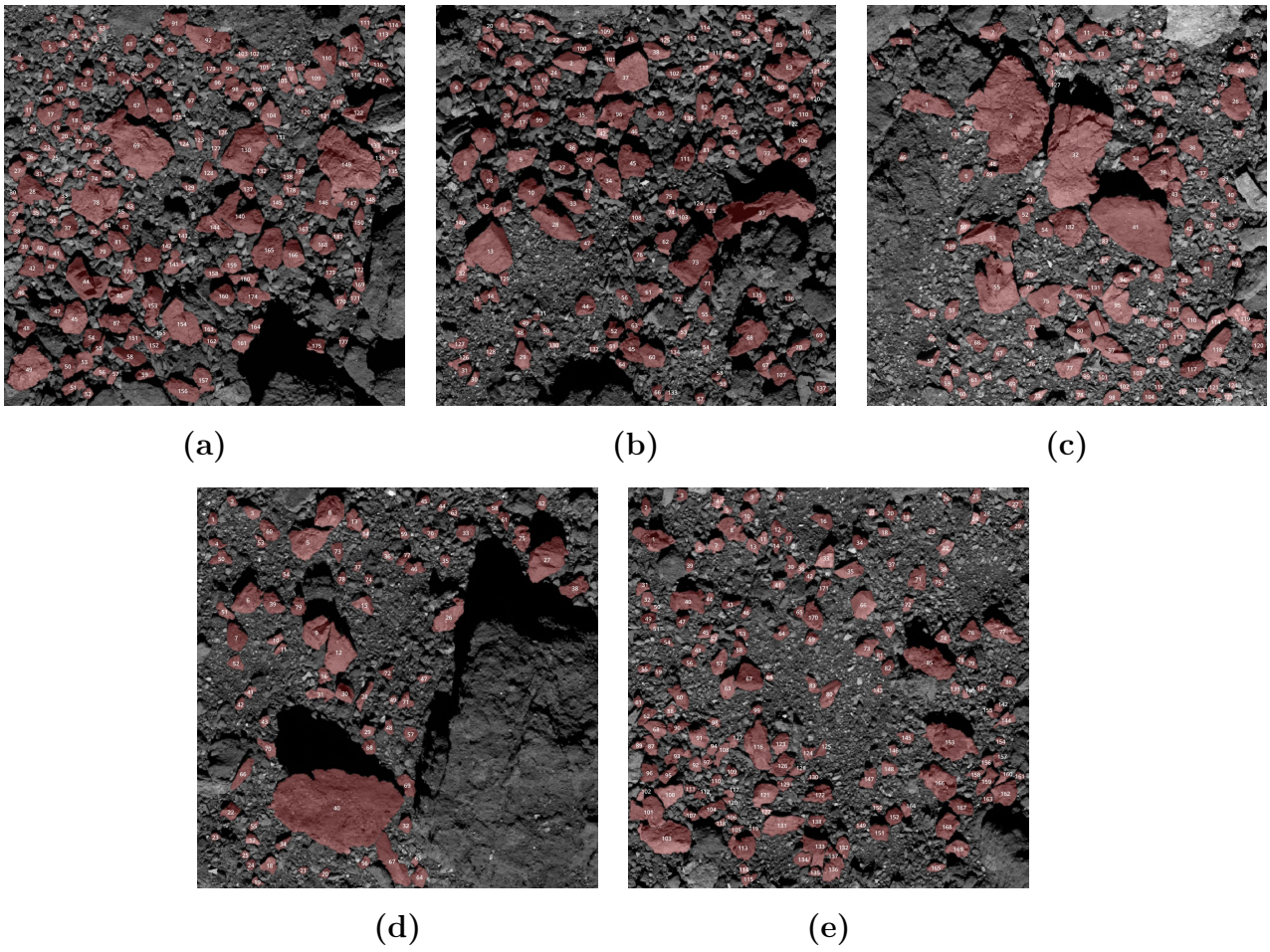

(a) **(b)** **(c)**

(d) **(e)**

Figure 27: The mapped boulders (red) from the Smooth 1 region. The numbers refer to individual boulder IDs that were assigned for tracking purposes only, image IDs: **(a)** 20191012T223409S486 **(b)** 20191012T223340S501 **(c)** 20191012T223103S875 **(d)** 20191012T222715S982 **(e)** 20191012T222650S984

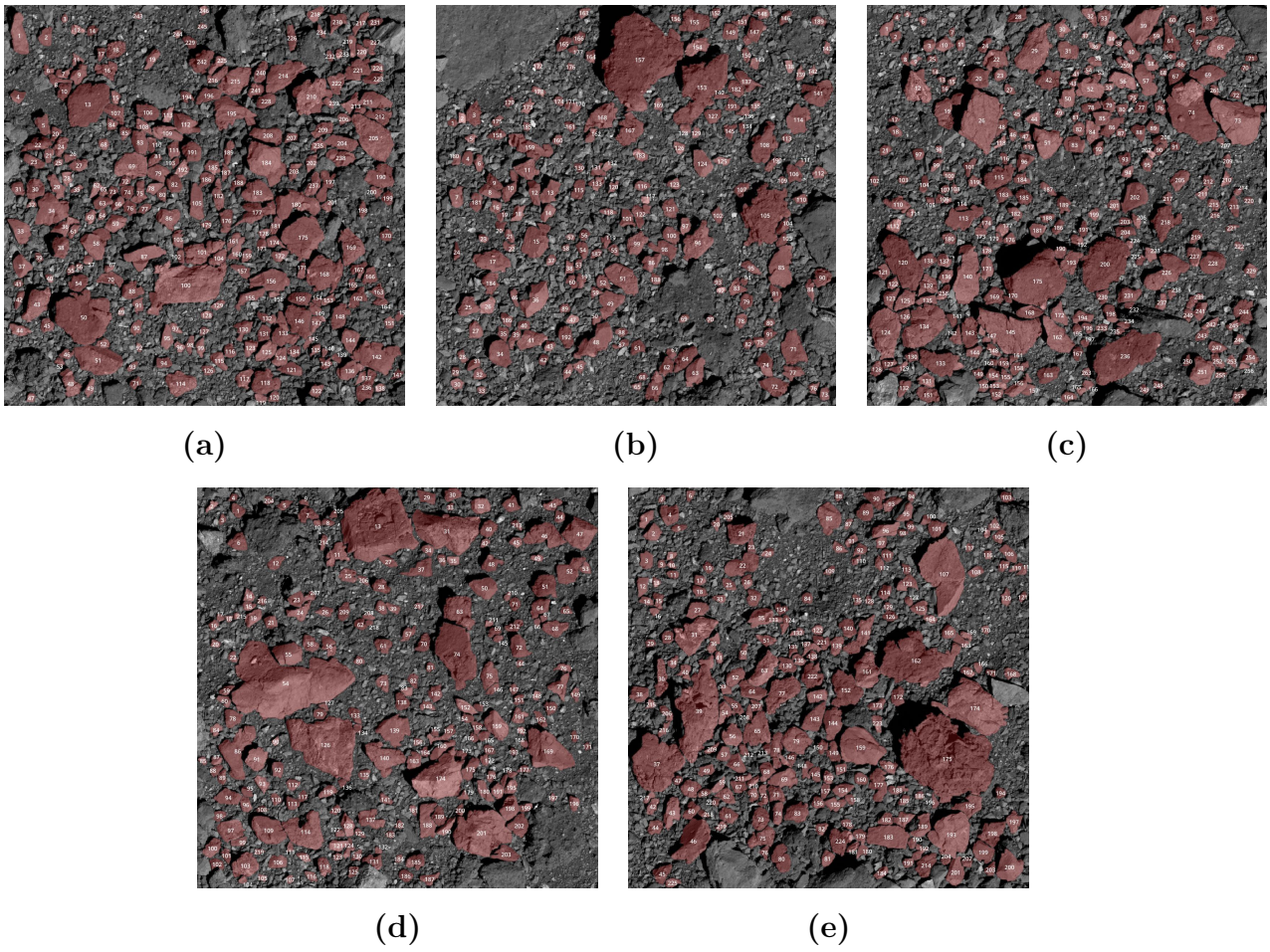

(a) **(b)** **(c)**

(d) **(e)**

Figure 28: The mapped boulders (red) from the Smooth 2 region. The numbers refer to individual boulder IDs that were assigned for tracking purposes only, image IDs:: **(a)** 20191026T223241S428 **(b)** 20191026T223125S701 **(c)** 20191026T222923S826 **(d)** 20191026T223039S912 **(e)** 20191026T222806S995

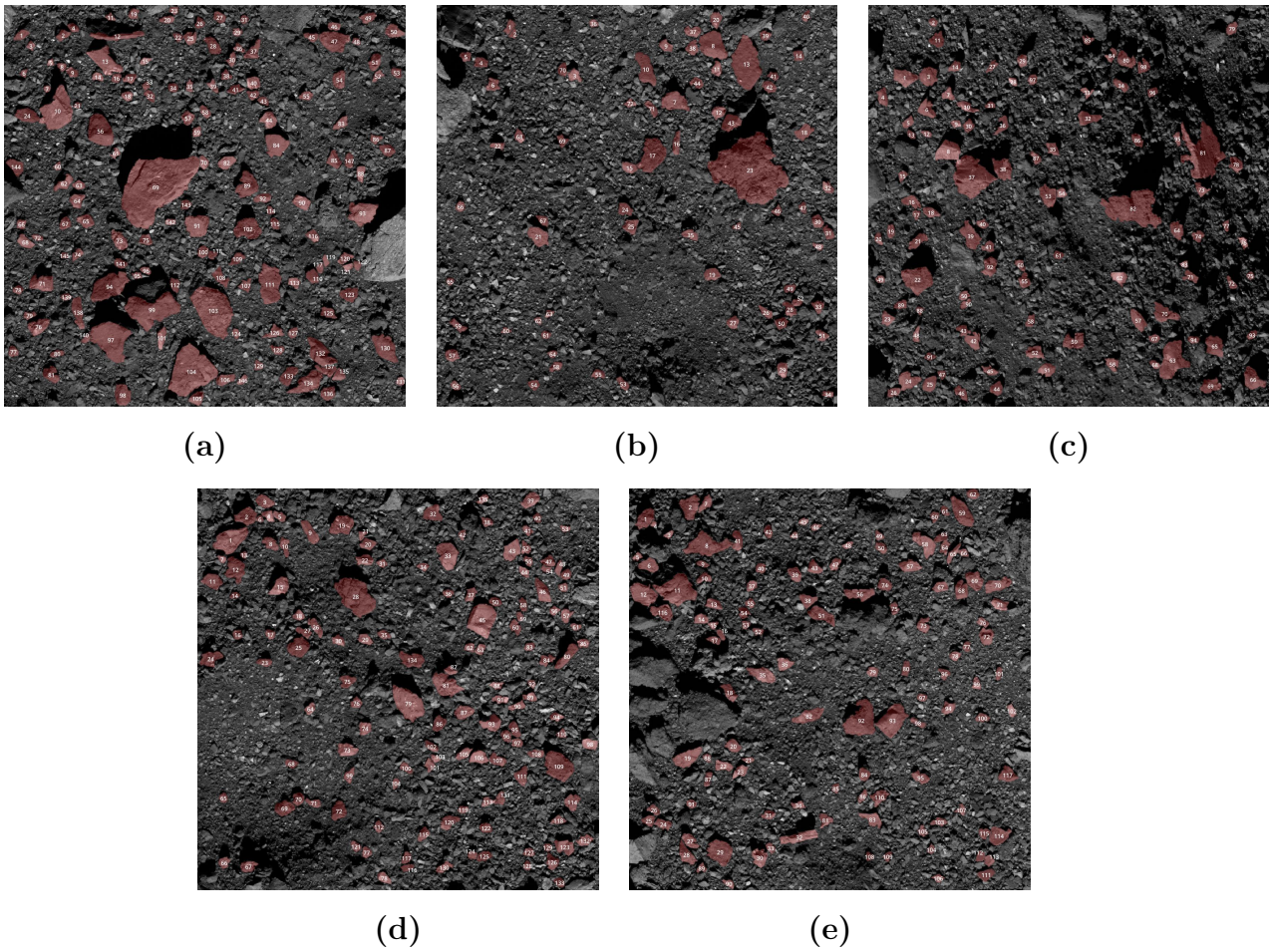

Figure 29: The mapped boulders (red) from the Smooth 3 region. The numbers refer to individual boulder IDs that were assigned for tracking purposes only, image IDs: **(a)** 20191005T193458S053 **(b)** 20191005T194314S115 **(c)** 20191005T200500S273 **(d)** 20191005T193926S463 **(e)** 20191005T194336S525

6.1.1 Number of boulders plotted

Table 5 shows the number of boulders I identified in each image, as well as the number of boulders that were assigned to each certainty level. The average size of all boulders in the Rugged Unit combined was (0.711 ± 0.48) m, and for the Smooth Unit, it was (0.579 ± 0.35) m.

Table 5: Number of plotted boulders in each region

Image ID	Region	Level 1	Level 2	Level 3	Total
20191026T220330S729	Rugged 1	119	55	4	178
20191026T220320S574	Rugged 1	99	41	4	144
20191026T220308S430	Rugged 1	111	63	16	190
20191026T220212S730	Rugged 1	134	59	11	204
20191026T213742S732	Rugged 1	117	50	5	172
	Total:	580	268	40	888
20191012T222715S982	Smooth 1	40	34	5	79
20191012T223340S501	Smooth 1	58	67	15	140
20191012T223103S875	Smooth 1	80	53	6	139
20191012T223409S486	Smooth 1	93	79	9	181
20191012T222650S984	Smooth 1	96	68	8	172
	Total:	367	301	43	711
20191005T202551S161	Rugged 2	26	25	5	56
20191005T202438S908	Rugged 2	39	29	4	72
20191005T202949S197	Rugged 2	74	47	13	134
20191005T202016S711	Rugged 2	48	43	7	98
20191005T203012S510	Rugged 2	43	15	4	62
	Total:	230	159	33	422
20191026T223125S701	Smooth 2	87	98	8	193
20191026T223241S428	Smooth 2	115	115	16	246
20191026T222923S826	Smooth 2	146	113	4	263
20191026T222806S995	Smooth 2	118	101	6	225
20191026T223039S912	Smooth 2	112	103	4	219
	Total:	578	530	38	1146
20191005T193228S655	Rugged 3	73	44	8	125
20191005T193048S900	Rugged 3	37	18	6	61
20191005T193407S925	Rugged 3	58	33	13	104
20191005T193034S211	Rugged 3	43	20	4	67
20191005T194948S256	Rugged 3	61	37	9	107
	Total:	272	152	40	464
20191005T194314S115	Smooth 3	31	38	3	72
20191005T200500S273	Smooth 3	36	52	10	98
20191005T194336S525	Smooth 3	57	57	3	117
20191005T193926S463	Smooth 3	70	63	2	135
20191005T193458S053	Smooth 3	96	48	3	147
	Total:	290	258	21	569

6.2 Boulder Size

After the mapping was completed and the data was extracted, the next step was to get an overview of it. An overview of the average boulder size and the average resolution can be seen in Table 6. I started by creating a boulder size histogram to assess how the boulder size (defined as the longest axis of the boulder) is distributed in the two units. The histogram can be seen in Figure 30a. In order to mitigate that the images have slightly different resolutions, I used a lower cut-off point of 0.3 m, as this was the smallest boulder plotted in the region with the worst resolution (Rugged 3). However, the area each of the regions cover is different as the images have different resolutions, so I also checked if the boulder count would show the same trend when studied per area. The area covered was approximated by converting the image area in pixels to km^2 by multiplying it with its resolution. As I used non-projected images, this is just an approximation, but since this was only done to check if the trend was similar when checked per area, I judged that an approximation was enough. The images in the Rugged had a total combined area of approximately 0.00287 km^2 and the Smooth Unit had one of 0.00244 km^2. The histogram that shows the boulder sizes per area can be found in Figure 30b.

Table 6: Average resolution and boulder size of each region investigated in this work.

Region	**Average resolution (cm/pxl)**	**Average boulder size (m)**
Rugged 1	1.26 ± 0.041	0.665 ± 0.38
Smooth 1	1.23 ± 0.0028	0.654 ± 0.39
Rugged 2	1.35 ± 0.0026	0.737 ± 0.63
Smooth 2	1.07 ± 0.0038	0.585 ± 0.34
Rugged 3	1.44 ± 0.0072	0.814 ± 0.46
Smooth 3	1.40 ± 0.0031	0.615 ± 0.32

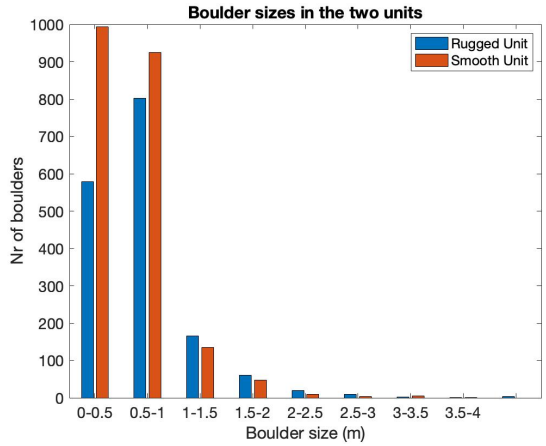

(a) Histogram of the boulder sizes in the two units that I mapped. The regions from the Rugged Unit are shown in blue and the regions from the Smooth Unit are shown in red.

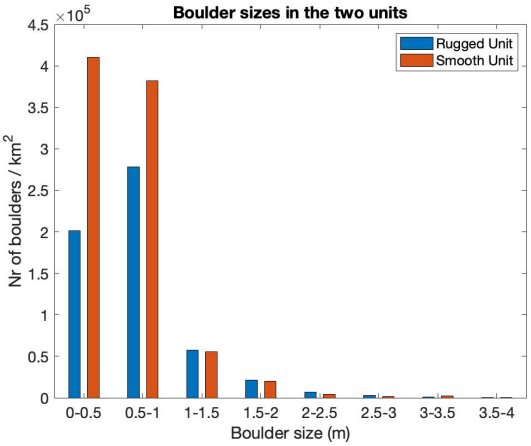

(b) Histogram of the boulder sizes in the two units per area. The regions from the Rugged Unit are shown in blue and the regions from the Smooth Unit are shown in red.

Figure 30: Histogram of boulder sizes as found when mapping and when studied per area.

After this, I created a cumulative frequency graph of the different regions. The graph is shown in Figure 31. Again, the boulder size is defined as the largest axis of the boulder. The plot shows the number of boulders per area. As can be seen, there does not seem to be a significant difference between the regions in terms of boulder size distribution. However, it is interesting to note that all regions have their largest boulder at around 3 to 4 meters, except for Rugged 2 that has one boulder at around 9 meters. The lack of other larger boulders are due to the fact that the images chosen have high resolutions of about 0.013 m/pixel, so their field of view is relatively small (less than 15 meters across), as discussed in subsection 4.1. This led to large boulders often being too large to fit completely in the image, which meant that they were not included in the map.

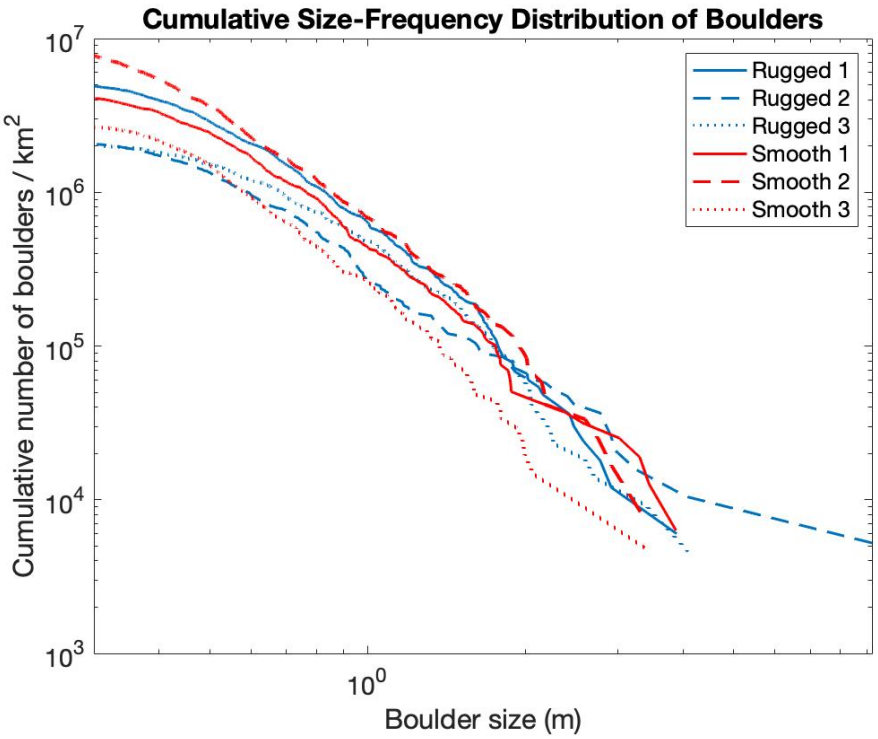

Figure 31: Cumulative size-frequency distribution of boulders in all six regions. The regions from the Rugged Unit are shown in blue and the regions from the Smooth Unit are shown in red.

6.3 Boulder Roughness

The first morphological feature I studied was the boulder roughness. I did this by looking at two shape factors, the solidity (S) and the circularity (C). Their equations can be found in Equation 4 and Equation 3 in section 3, respectively. Note that, as shape factors are size-independent, boulders of all sizes were included. Figure 32a shows the average solidity plotted against the average boulder size in the six regions. Boulder size is defined as the longest axis of the boulder. Figure 32b shows the average circularity plotted against the average boulder size for the six regions. Finally, Figure 33 shows the average circularity plotted against the average solidity in the six regions. The average solidity for the Rugged Unit was 0.925 $\pm$ 0.044 and for the Smooth Unit it was 0.931 $\pm$ 0.045. The average circularity for the Rugged Unit was 0.720 $\pm$ 0.11, and for the Smooth Unit it was 0.735 $\pm$ 0.11.

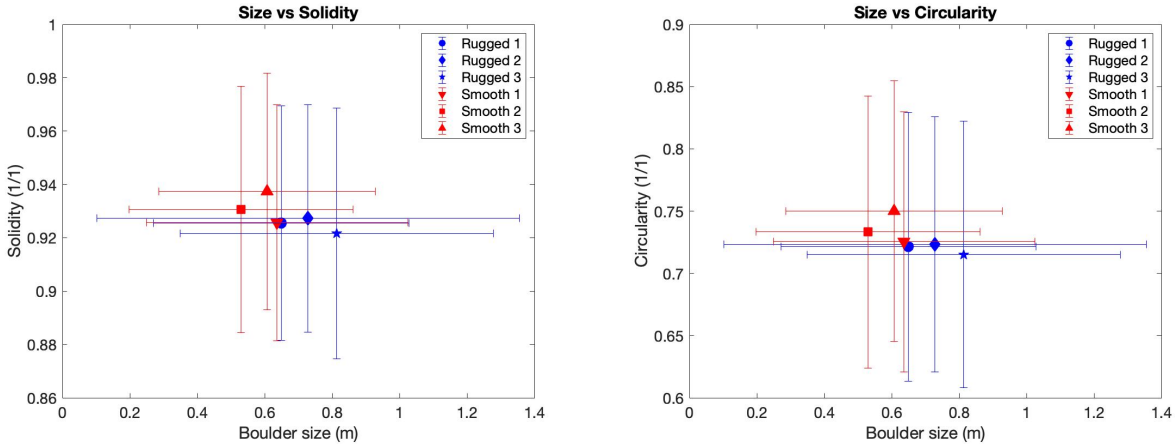

(a) The average boulder size against the average solidity of the six regions. The individual points show the average of all boulders in one region and the one sigma standard deviation.

(b) The average boulder size against the average circularity of the six regions. The individual points show the average of all boulders in one region and the one sigma standard deviation.

Figure 32: Average boulder size against average solidity and average circularity.

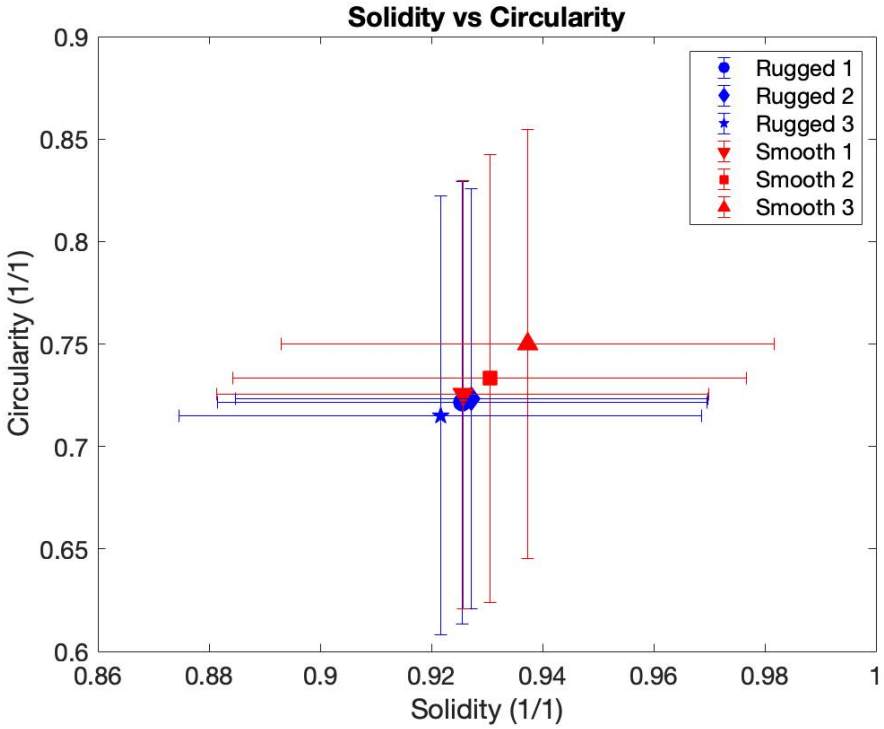

Figure 33: The average solidity against the average circularity of the six regions. The individual points show the average of all boulders in one region and the one sigma standard deviation.

6.4 Boulder Compactness

Next, I wanted to know about the compactness of the boulders. I wanted to know if the boulders tend to have a compact shape, or if they tended to be more elongated. I studied this by looking at the two shape factors elongation (E) and roundness (R). Their equations can be found in Equation 5 and Equation 7 in section 3, respectively. Figure 34a shows the average elongation plotted against the average boulder size in the six regions. Figure 34b shows the average roundness plotted against the average boulder size for the six regions. Figure 35 shows the average roundness plotted against the average elongation in the six regions. The average elongation of the Rugged Unit was 0.706 ± 0.17, and for the Smooth Unit it was 0.714 ± 0.16. The average roundness of the Rugged Unit was 0.645 ± 0.17, and for the Smooth Unit it was 0.656 ± 0.16.

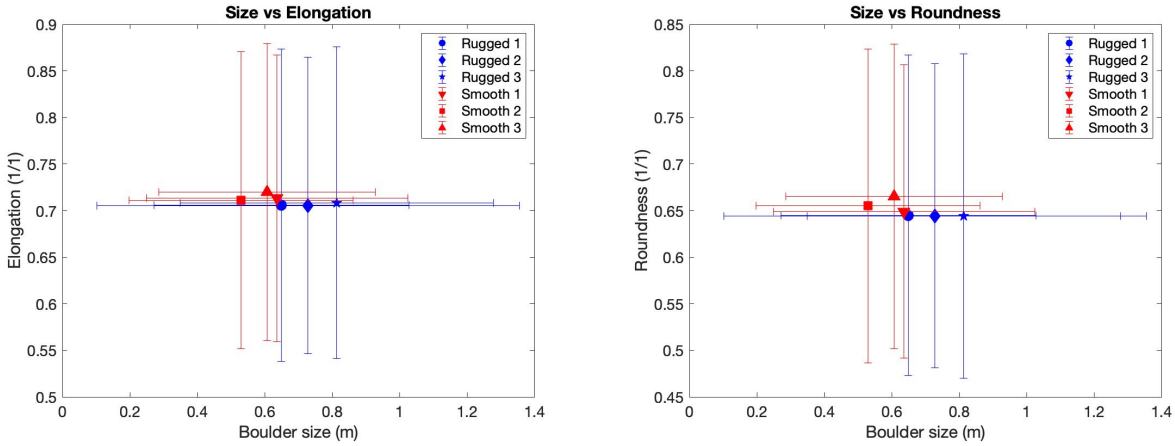

(a) The average boulder size against the average elongation of the six regions. The individual points show the average of all boulders in one region and the one sigma standard deviation.

(b) The average boulder size against the average roundness of the six regions. The individual points show the average of all boulders in one region and the one sigma standard deviation.

Figure 34: Average boulder size against average elongation and average roundness.

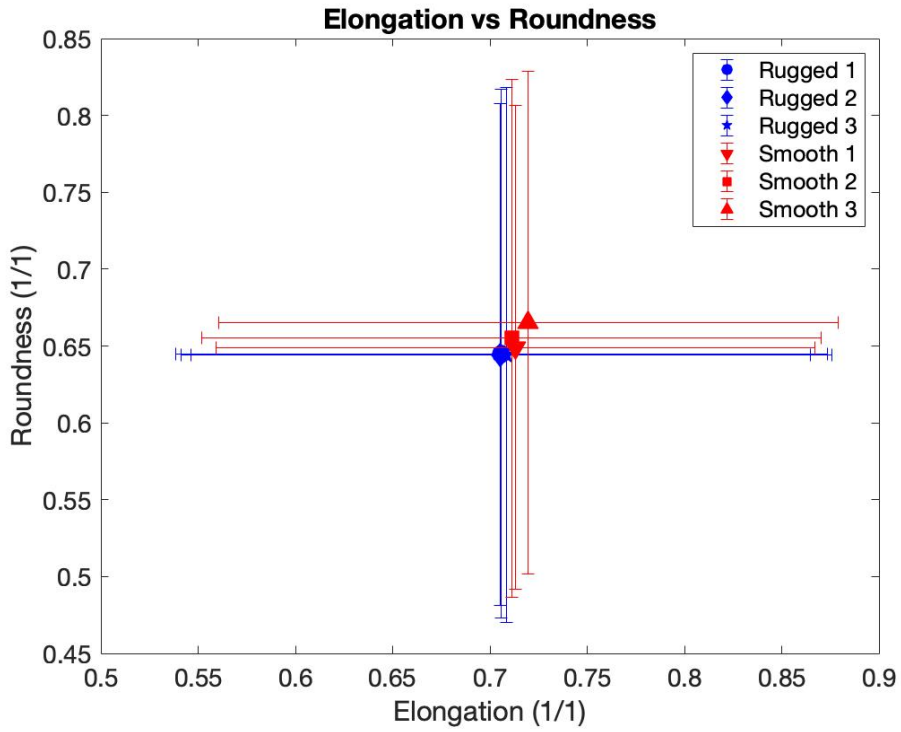

Figure 35: The average elongation against the average roundness of the six regions. The individual points show the average of all boulders in one region and the one sigma standard deviation.

6.5 Boulder roughness compared to boulder compactness

After looking at both the boulder roughness and the boulder compactness individually, I compared them with each other. For this, I plotted the circularity against the roundness, as they were the parameters with the largest range in values. The resulting graph can be seen in Figure 36.

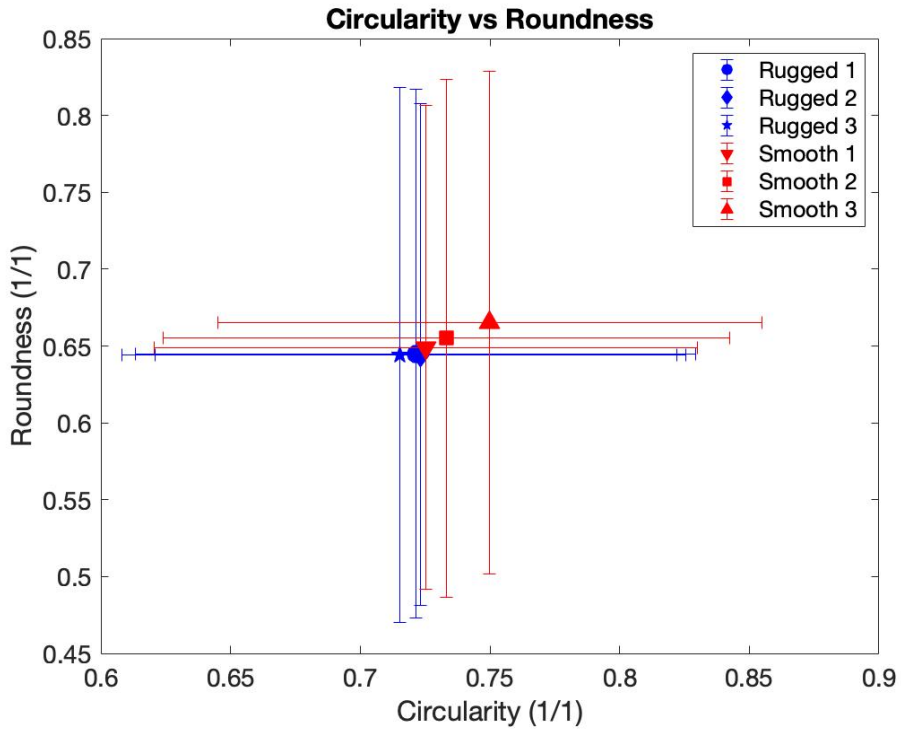

Figure 36: The average circularity (a roughness parameter) against the average roundness (a compactness parameter) of the six regions. The individual points show the average of all boulders in one region and the one sigma standard deviation.

6.6 Shape factors compared to boulder size

Finally, I looked into how the different shape factors relate to the size of the individual boulders. Figure 37 shows how the shape factors describing boulder roughness relate to the size of the boulder, and Figure 38 shows how the shape factors describing boulder compactness relate to the size of the boulder. These graphs are cut off at 4.5 meters boulder size despite one boulder in the Rugged 2 region being 9.19 m for legibility. Each point represents one mapped boulder.

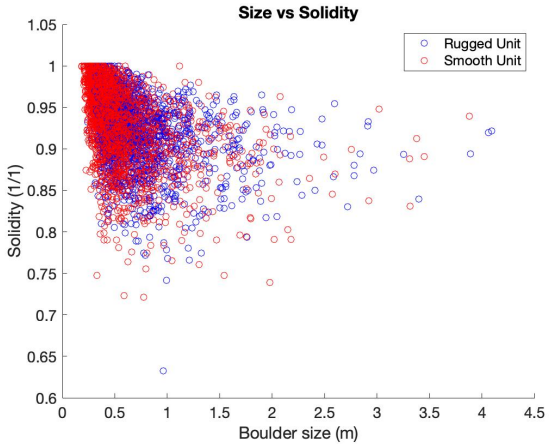

(a) The boulder size against the solidity of individual boulders.

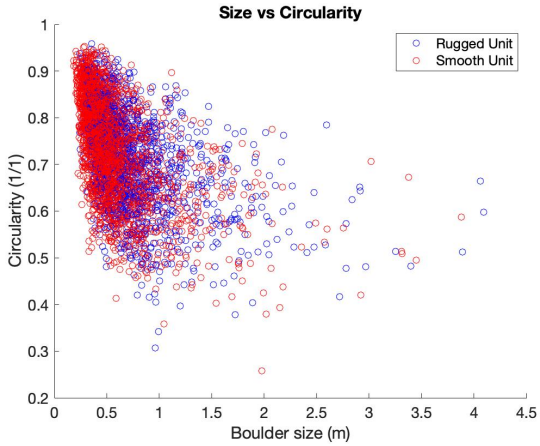

(b) The boulder size against the circularity of individual boulders.

Figure 37: Boulder size against the roughness shape factors, solidity and circularity.

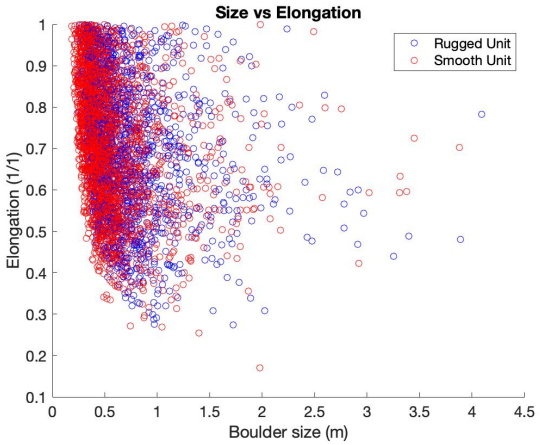

(a) The boulder size against the elongation of individual boulders.

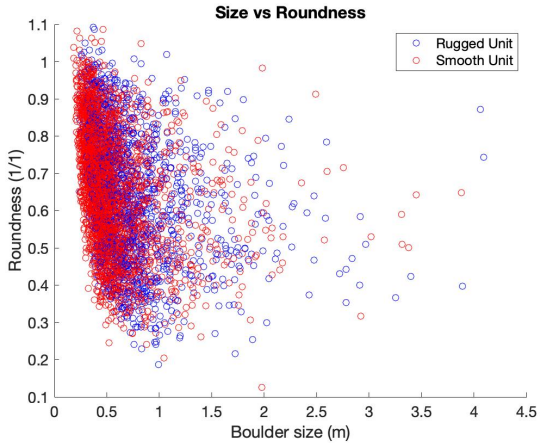

(b) The boulder size against the roundness of individual boulders.

Figure 38: Boulder size against the compactness shape factors, elongation and roundness.

7 Discussion

In this section, I will discuss the results found in this work, and compare them to previous published results. I will discuss the boulder size, compactness, and roughness, and see how they relate to each other, and if there is difference between the two geologic units, as well as seeing if my results are similar to that of other works.

In general, there are more and smaller boulders in the Smooth Unit, which can be seen in Figure 30. As mentioned in subsubsection 6.1.1, the Rugged Unit has 1774 boulders mapped with an average size of (0.711 ± 0.475) m, and the Smooth Unit has 2426 boulders mapped with an average size of (0.579 ± 0.35) m. This is in disagreement with the findings of Jawin et al. (2022) [14], which stated that the Smooth Unit is "boulder poor" compared to the Rugged Unit. However, they did not do detailed analysis of boulders smaller than 20 meters, explaining the difference to my results. When studying Figure 30b, it can be seen that in the 0 to 1 m range, the Smooth Unit has more boulders, but over 1 m, there is no distinct difference between the two units. However, as mapping of boulders is a manual process that depends on many variables (e.g. observational conditions, quality of data sets, mapping experience), other teams may find different size histograms even if they were to study the same body. The boulder size can also be seen in the plots showing the different shape factors plotted against boulder size (Figure 32a, Figure 32b, Figure 34a and Figure 34b). In these plots, it can be seen that the average boulder size of all smooth regions are smaller than the average boulder size of all rugged regions. By looking at the error bars, it can be seen that the rugged regions have a wider range of boulder sizes.

Something worth noting is that the region with the smallest boulders is the Smooth 2 region, and the region with the largest boulders is the Rugged 3 unit. Smooth 2 is the region with the best resolution, and Rugged 3 is the region with the worst resolution. This could contribute to why fewer small boulders are found in the Rugged 3 region, since then the boulders that fit the "at least 15 pixels across" criteria would be bigger. However, Table 6 shows the average resolution for each of the regions and as can be seen in the table, even though Smooth 2 has the best resolution and Rugged 3 has the worst, the remaining images have fairly similar resolutions. This, combined with the fact that the average largest mapped boulder in each of the rugged regions is bigger than the average largest mapped boulders in the smooth regions, implies that the statement that the boulders in the Smooth Unit are generally smaller compared to the boulders in the Rugged Unit is valid. Furthermore, in

Figure 30, I only plotted boulders larger than 0.3 m, as that was the smallest boulder in the Rugged 3 region, and it can still be seen that the Smooth Unit has more smaller boulders than the Rugged Unit. One of the arguments that Jawin et al. (2022) [14] used to distinguish the Rugged Unit from the Smooth Unit was indeed that the Rugged Unit has more large boulders, which is in agreement with my findings. However, they only looked at boulders larger than 20 m, which is a lot larger than the largest boulders I mapped (the largest boulder I mapped was 9.2 m and the second largest was 4.1 m). The images I have used in this work are much higher resolved and a boulder of that size would not fit into the image. On Bennu, the difference in boulder sizes over the surface is believed to be partly created by large-scale surface creep [2]. Regolith and smaller boulders migrate towards the equator (which is where the Smooth Unit mainly is), while larger boulders do not get as moved by surface creep and stay at higher latitudes (which is where the Rugged Unit mainly is). This is in agreement with my observation of smaller boulders populating the Smooth Unit.

7.1 Boulder Roughness

As can be seen in Figure 32a to Figure 33, the boulders in the smooth regions are generally slightly more solid and circular, which means that they are less rough. As mentioned in section 3, a rough boulder will have lower solidity and circularity, while a smoother one will have values close to one. As the Smooth Unit is suggested to be older than the Rugged Unit [14], the boulders there could be smoother due to having been exposed to erosive and weathering processes on the surface for a longer period of time [4]. On Bennu such processes include surface creep, micrometeorite impacts or thermal weathering [14]. It can also be seen that the solidity and circularity follow a linear trend when plotted against each other. This is expected as they both are a way to measure boulder roughness. So a boulder with high solidity should also have high circularity. Although we do see that the smooth regions have slightly higher solidity and circularity, and thus are less rough than the rugged regions, the difference is not statistically significant, and there is a great amount of overlap between values in the two regions. This illustrates that the definition of Rugged and Smooth Units is linked to the boulder size but not the boulder shape. As boulder roughness is uniform over the surface of Bennu, this implies that processes that may influence boulder roughness, such as micrometeorite impacts and thermal weathering [26], are more efficient than particle migration that exposes fresh material that may possess different roughness, which is a gradual process on Bennu [2]. This is in agreement with the findings of Delbo et al. (2022) [9], as they found that thermal fracturing on Bennu only takes $10^4 - 10^5$ years, which is comparatively

shorter than mass movement processes.

Szabo et al. (2015) [35] investigated solidity and circularity of what they identified as "angular" and "rounded" pebbles on Mars, and Cambianica et al. (2019) [4] investigated solidity and circularity of the comet 67P. Figure 39 show a comparison of their values with the values I found for Bennu's two geologic units in this work. As can be seen, the values for solidity are similar, however, 67P and the Mars rounded grains possess a higher circularity. This is not unexpected, as Mars is a planet and 67P is a comet while Bennu is an asteroid, so the processes altering circularity and solidity vary significantly. On Mars and 67P, fluvial [35] and sublimation [26] processes affect boulder roughness respectively, processes which are not present on asteroids. It can also be seen that the error bars for Bennu are wider than for Mars and 67P, which indicates that Bennu has more diverse boulder shapes than the other two bodies.

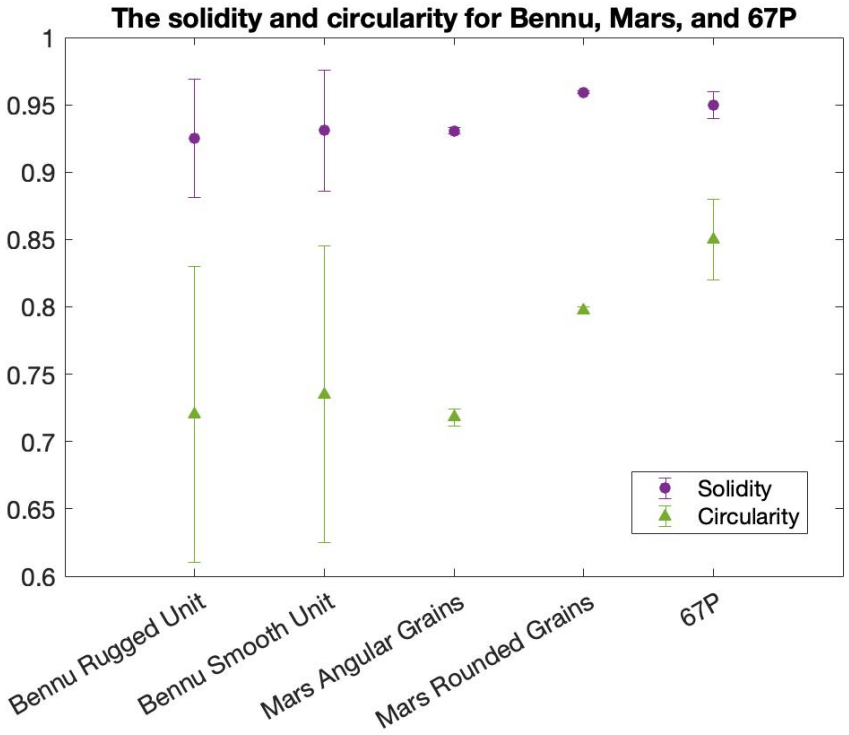

Figure 39: Comparison of the solidity and circularity of Bennu's Smooth and Rugged Unit as identified in this work, with that of angular and round grains on Mars [35] and the comet 67P [4].

7.2 Boulder Compactness

As can be seen in Figure 34a to Figure 35, the boulders in the smooth regions are slightly more compact than in the rugged regions. This can be seen because both the elongation and the roundness is generally higher for the smooth regions than for the rugged regions. As mentioned in section 3, an elliptically shaped boulder will have low elongation and roundness, while a more compact one will have values close to one. Here, it can also be seen that boulder elongation and roundness follow a fairly linear trend when plotted against each other. Again, this is to be expected as they both are a way of measuring if a boulder is more elongated or compact. Interestingly, for the rugged regions, we can see that there is very little variation in elongation and roundness. As with the boulder roughness, even though we do see that the boulders in the smooth regions are slightly rounder compare to the boulders in the rugged regions, the difference is not statistically significant, and we see a significant overlap in values here as well.

As mentioned in subsection 6.4, the elongation of the Rugged Unit is 0.706 ± 0.17, and for the Smooth Unit it is 0.714 ± 0.16. Laboratory experiments of impact fragments caused by a catastrophic disruption have found that the fragments usually have an elongation of around 0.7 [24], so my results match these laboratory experiments well. This laboratory derived value is based on catastrophic collisions and does not take into account other phenomena that can affect boulder shape, such as impact gardening and thermal fracturing. Thus my results agree with the hypothesis that the boulders on Bennu are remnants of the catastrophic collision that created the asteroid. Figure 40 shows the distribution of boulder elongation derived in my work, as well as in laboratory experiments performed by Capaccioni et al. (1984) [5]. In their work, they found an average elongation of 0.72, so it matches my results well. The shape of the distribution is also similar to my work, with the majority of boulders being in the 0.7 - 0.8 bin for both units. However, my distribution presents a wider spread of boulder elongation, with both the 0.5 - 0.6 and 0.9 - 1.0 bin containing relatively more boulders than in the laboratory results. This could be explained by the fact that there have been other processes affecting the boulders' shape on Bennu, such as impact and thermal fracturing, after the original catastrophic collision. The work done by Capaccioni et al. (1984) [5] focuses on hypervelocity impacts only, so these other processes could explain the discrepancies in the boulder elongation distributions. The fact that there are more boulders in the 0.9 - 1.0 bin in my work compared to Capaccioni et al. (1984) [5] could also be explained by Bennu having weathered boulders that became more compact (and thus have a higher elongation value)

due to weathering effects over the years.

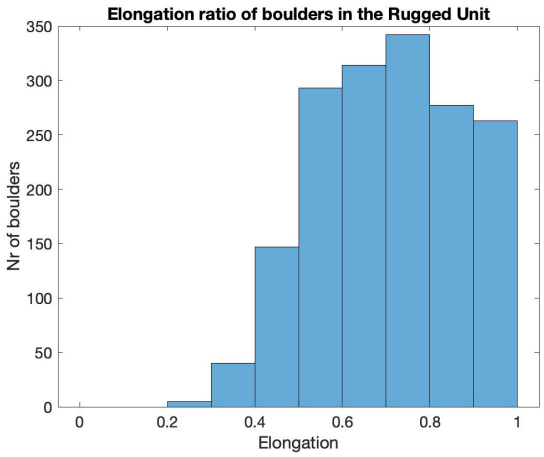

(a) Histogram of the elongation distribution for the Rugged Unit.

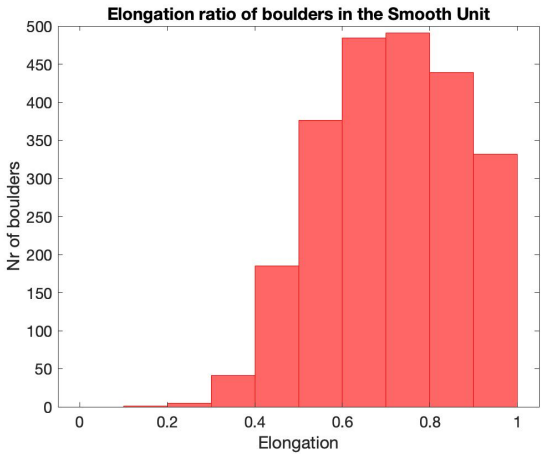

(b) Histogram of the elongation distribution for the Smooth Unit.

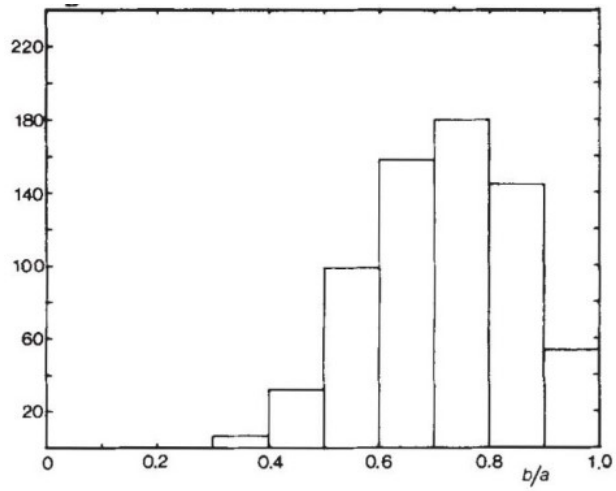

(c) Histogram of the laboratory results found by Capaccioni et al. (1984) in their experiments on impact velocity fragmenting [5]

Figure 40: Histograms showing the elongation ratios found in this study for Bennu's Rugged and Smooth geological units compared to laboratory results [5].

Michikami et al. (2016) [24] also performed laboratory experiments investigating the fragments created from high velocity impacts. In their experiments, they tested impacts with different forces to simulate different processes. Type 1 to Type 3 impacts were done with lower impact velocity to stimulate non-catastrophic impacts such as cratering, while Type 4 has a higher impact velocity in order to simulate a catastrophic impact. Their resulting distribution of elongation values can be seen in Figure 41. Type 2 and Type 3 had a

mean elongation of 0.71, which is nearly identical to my average values of 0.706 ± 0.17 for the Rugged Unit and 0.714 ± 0.16 for the Smooth Unit. By looking at the shape of the distribution, my elongation distributions are most similar to that of Type 3 impacts. This would imply that the boulders on Bennu are not formed by a catastrophic impact, but rather by another fragmentation process. However, other laboratory results suggest that a mean elongation of catastrophic impacts could vary between 0.70 and 0.74 [23], and as mentioned previously, laboratory results may disregard processes that occur on the actual bodies, such as micrometeorite impacts and thermal weathering, that can effect boulder shapes. Just studying a histogram distribution may also not be the most reliable way to deduce results, and it is expected that a rubble-pile asteroid like Bennu has a majority of boulders created by the catastrophic impact [16].

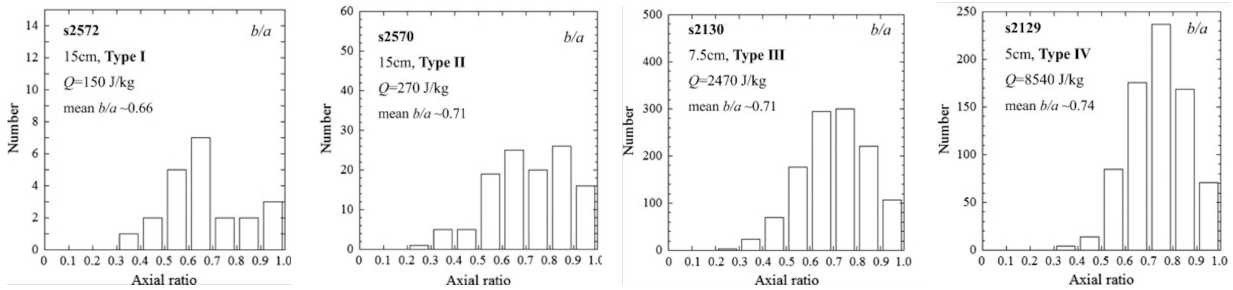

(a) Type 1 impact test. (b) Type 2 impact test. (c) Type 3 impact test. (d) Type 4 impact test.

Figure 41: The distributions of fragment elongation of different impact tests performed by Michikami et al. (2016) [24]. The types refer to how much force was used in the impact experiment, representing different kinds of impacts. In the legends, the first entry is the name of the specific experiment, the second entry is the size of the target and the identified type of impact, the third (Q) is the kinetic energy of the projectile per unit target mass, and the fourth entry (mean b/a) is the elongation of the resulting fragments.

Figure 42 show a comparison of the elongation I found for Bennu's two geological regions with the average elongation of asteroid Ryugu found by Michikami et al. (2019) [23] and the average elongation of asteroids Eros and Itokawa found by Michikami and Hagermann (2021) [22] (although no errors were given for these bodies, which can make comparison difficult). As can be seen, my values for Bennu, and their value for Eros fall within the 0.70 to 0.74 range found in laboratory experiments, while their values for Itokawa and Ryugu are below the experimental range. However, something to keep in mind is that the boulders I mapped were a lot smaller than the boulders they mapped. For Eros, they only mapped boulders

that were greater than 30 meters, and for Ryugu and Itokawa, they only mapped boulders that were larger than 5 meters [22]. This could be a potential error source when comparing my results to theirs.

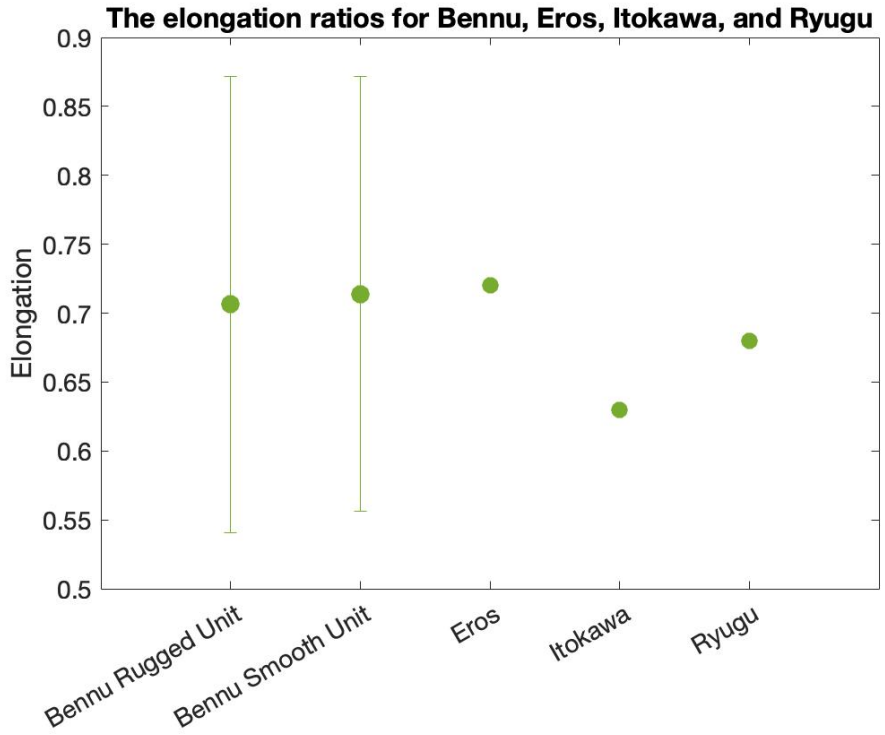

Figure 42: Comparison of the boulder elongation of Bennu's Smooth and Rugged Unit as identified in this work, with the mean elongation ratio of asteroids Ryugu [23], Eros and Itokawa [22].

7.3 Boulder roughness compared to boulder compactness

As can be seen in Figure 36, there is a greater variation in the roughness of the boulders (i.e. the circularity) than the compactness of the boulders (i.e. the roundness). This means that the compactness of the boulders are not as affected by which region they are found in as the roughness of the boulders is. However, even though the difference in boulder compactness (roundness) is similar between the two regions (0.645 $\pm$ 0.17 for the Rugged Unit and 0.656 $\pm$ 0.16 for the Smooth Unit), it can be seen that the smooth regions have slightly higher roundness values than the rugged regions, which means that there are generally more compact boulders within the smooth regions, as discussed in subsection 7.2.

On the other hand, there is a greater variation between the regions when it comes to boulder

roughness. As discussed in subsection 7.1, the smooth regions have higher values for the shape factors relating to roughness (circularity), which indicates that they are smoother.

Overall, we can see that both roughness and compactness values are slightly higher in the smooth regions. This indicates that the smooth regions generally have less elongated and less rough boulders than the rugged regions. However, as mentioned in the previous subsections, this difference is not statistically significant between the two geological regions. Both units contain a wide variety in both compactness and roughness that overlap significantly. From this I infer that the boulder morphology is relatively uniform over the surface of Bennu, which may mean that the mechanical properties associated with boulder shapes, such as stiffness, strength and volumetric properties [33] (as discussed in section 3), are similar in the two units. Although the two units are geologically distinct, the boulder morphology is homogeneous.

7.4 Shape factors compared to boulder size

In Figure 37b, we can see that small boulders tend to be more smooth than larger ones. Something to keep in mind when studying how shape factors relate to boulder size is that the images with better resolution show more smaller boulders, as discussed earlier in the Discussion section. However, we can see in Figure 32b that the region with the highest circularity is Smooth 3, even though the region with the best resolution is Smooth 2 (see Table 6). This means that the circularity is not uniquely linked to the image resolution and I can still make comparisons with boulder size even though the resolution of the images is different.

When assessing boulder circularity, it is important to note that the small boulders will not have as detailed outlines as larger ones. Large boulders allowed me to trace their outline very accurately when using the same zoom as when looking at the smaller boulders. To avoid this as much as possible, I set a pixel resolution limit and did not outline any boulders that were smaller than 15 pixels across, as mentioned in section 4. However, this procedure may not have removed the entire bias and it is still possible that the results are affected by this, potentially influencing the observation that the smaller boulders are smoother and rounder.

Figure 38a shows that the elongation seems to be the least dependent on boulder size of the shape factors I studied. We can see some boulders with an elongation of 1 (meaning that the minor and the major axes of the boulder are the same size) when looking at the larger

boulders as well. This indicates that whether a boulder is elongated or not does not seem to be as affected by their sizes as their roughness is. In other words, we can find some compact boulders at larger sizes as well as smaller, while smooth boulders tend to be mostly found in the small sizes. Interestingly, Michikami and Hagermann (2021) [22] also found a trend of smaller boulders generally having slightly larger elongation than larger boulder in their work on asteroids Eros and Itokawa (see Figure 43). Michikami et al. (2019) [23] found this trend for asteroid Ryugu as well. However, as previously mentioned, they looked at larger boulders than me (they looked at boulders larger than 30 meters for Eros and boulders larger than 5 meters for Itokawa [22] and Ryugu [23]), so it could be that this effect is more pronounced when looking at larger boulders. Something worth mentioning is that I saw slightly larger elongation values for the smooth regions, as discussed in subsection 7.2, and the smooth unit has smaller boulders. So although the difference is not that pronounced, I do see a slight increase in elongation in the regions with smaller boulders.

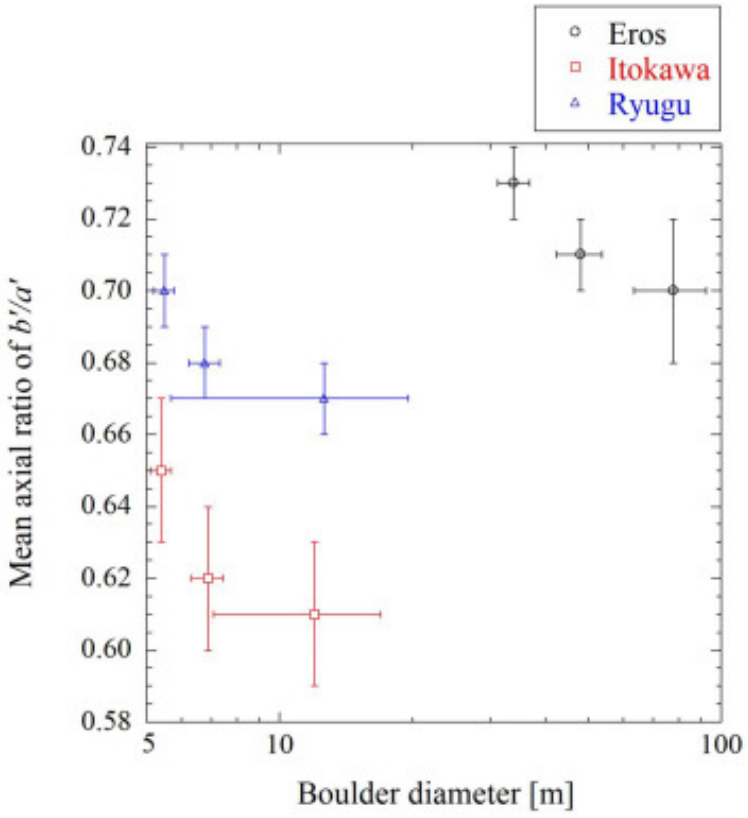

Figure 43: Elongation (mean axial ratio of b'/a') against boulder size for three representative size bins on asteroids Eros, Itokawa, and Ryugu from [22].

Two of the main processes that alter boulder roughness are micrometeorite impacts [4] and

thermal erosion [10]. Both processes can either make the boulders rougher or more smooth depending on the scale. For micrometeorite impacts can either remove sharp corners which has a smoothing effect [4], or they can remove parts of an already smooth boulder (e.g. by creating a crater [1]), thus making it rougher. A similar situation can be found for thermal erosion: it can either remove sharp edges of a boulder by cracking them off [10], making the boulder smoother, or it can lead to the boulder cracking into two or more pieces, which can create new sharp edges. This is illustrated in Figure 44.

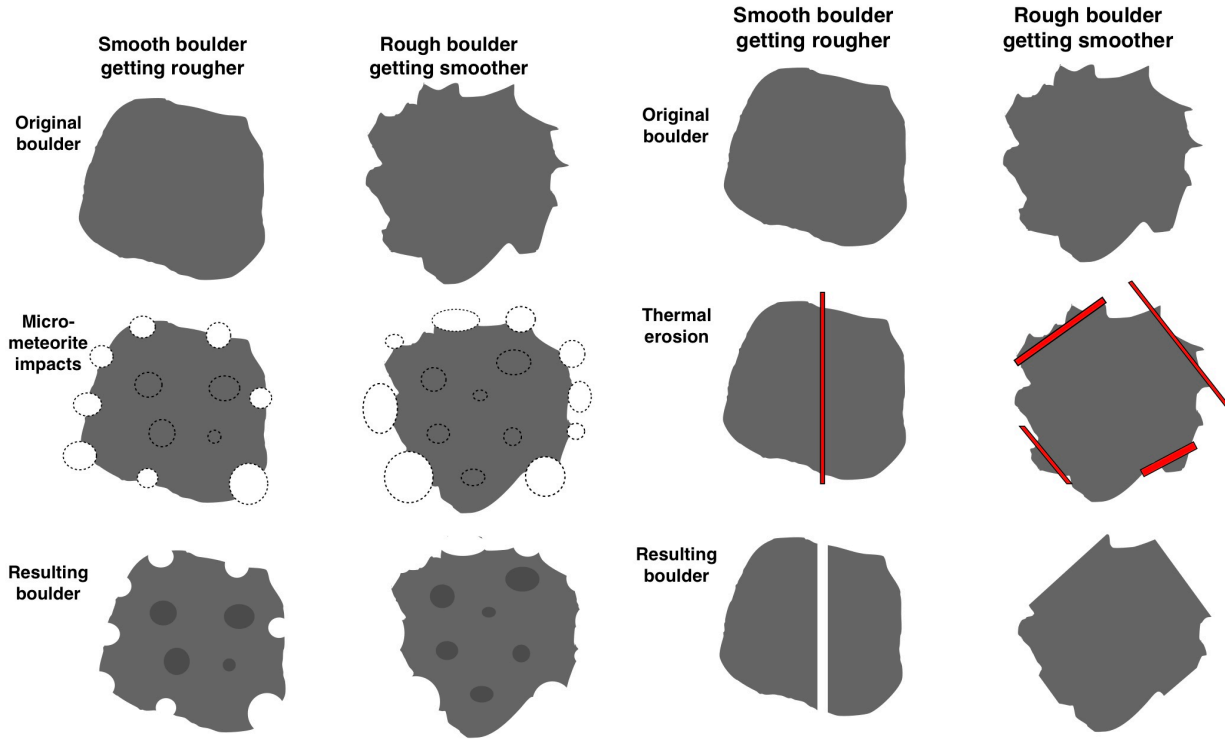

(a) Illustration showing the possible effects of micrometeorite impacts. The first row illustrates the original boulders (grey shapes), one smooth and one rough. The dotted circles in the second row illustrate micrometeorite impacts removing parts of the edges. The third row illustrates the resulting boulder after the impacts. The smooth boulder has gotten rougher and the rough boulder has gotten smoother.

(b) Illustration showing the possible effects of thermal erosion. The first row illustrates the original boulders (grey shapes), one smooth and one rough. The red lines in the second row illustrate thermal erosion cracking the boulder and removing parts of the edges. The third row illustrates the resulting boulder. The smooth boulder has become two boulders with sharp edges and the rough boulder has gotten smoother.

Figure 44: Illustration of the possible effects of micrometeorite impacts and thermal erosion.

As mentioned, the Smooth Unit contains more small boulders, which are smoother. Larger boulders in both units tend to be rougher (see Figure 32b), suggesting that on a larger scale, the weathering processes appear to make boulders rougher (e.g. by splitting or cratering), while on smaller scales, they seem to make them smoother (e.g. by removing sharp edges). Transportation of boulders can also lead to them becoming smoother as well as size segregated [35]. Because the Smooth Unit is older than the Rugged Unit, the boulders there have had a longer time to experience erosion and transport, which may contribute to why there are more small, smooth boulders. Although small, smooth boulders exist in both units, it is possible that the prolonged exposure to erosive processes in the Smooth Unit contributed to a comparatively large amount of small, smooth boulders. Small boulders are also easier to move, so they could potentially have moved more, which would also contribute to explaining why small boulders tend to be smoother in both units [15].

7.5 Potential error sources

Since the mapping was done by hand, there were some potential error sources. My tracing may not be the exact shape of the actual boulder. I mitigated this by only tracing boulders that were larger than 15 pixels across their smallest axis, so that enough detail could still be made out, and by using images with good resolution so I could see the boulders in more detail.

The shapes of the boulders might be off due to phenomena in the image as well, as mentioned in subsection 5.1. Things like shadows that either hid part of the boulder or made its shape unclear, boulders laying close or on top of each other so that their individual shapes can be hard to determine, regolith burying part of the boulder, or cracks that were hard to determine if it had split a boulder completely in two or not were all issues I had to deal with while mapping. As mentioned, the way I mitigated this was to assign a certainty level between one and three depending on how sure I was of the mapped outline. But since these certainty levels were also assigned manually by me, this could also be a potential error source.

As mentioned in section 5, I thought that the solar incidence angle and the emission angle might also be potential issues that would lead to me mapping the boulders incorrectly. This I mitigated by doing the investigations described in section 5, to try to determine if they introduced too big of a bias, which they do not.

8 Conclusion

I studied the boulder morphology of the two geologic units (one Smooth Unit and one Rugged Unit) on the asteroid Bennu found by Jawin et al. (2022) [14]. I did this by mapping boulders found on Bennu's surface in six different regions, three in the Smooth Unit and three in the Rugged Unit. I investigated boulder roughness by looking at the shape factors circularity and solidity, and boulder compactness by looking at the shape factors elongation and roundness.

I found that the Smooth Unit tended to have slightly smoother and rounder boulders than the Rugged Unit, but the difference was not statistically significant. This implies that boulder morphology is relatively uniform over the surface of Bennu, also indicating that the mechanical material properties associated with the boulder shape, such as stiffness, strength, and volumetric properties [33], are similar in the two units. Although the units are geologically distinct, the boulder morphology is homogeneous. I found that the elongation values agree well both with laboratory impact experiments and with studies done on other bodies, which indicates that the regolith was created by the catastrophic impact that created Bennu.

Lastly, I found that in general, smaller boulders tended to be more smooth than larger boulders, and that the Smooth Unit had both more and smaller boulders. As the Smooth Unit is the oldest [14], this indicates that weathering processes that smooths boulders are more efficient than processes that roughen them.

8.1 Future work

Future work that could be done on boulder morphology on Bennu includes expanding my work to look at more regions, since I only studied six regions in total. It could also be interesting to study the effect of image resolution on boulder mapping. Furthermore, comparing the shape factors I investigated with other asteroids could be interesting, as that is a field where not that much work has been done.

References

[1] R-L Ballouz et al. "Bennu's near-Earth lifetime of 1.75 million years inferred from craters on its boulders". In: *Nature* 587.7833 (2020), pp. 205–209. DOI: 10.1038/s41586-020-2846-z.

[2] OS Barnouin et al. "The formation of terraces on asteroid (101955) Bennu". In: *Journal of Geophysical Research: Planets* 127.4 (2022), e2021JE006927. DOI: 10.1029/2021JE006927.

[3] SJ Bus and RP Binzel. "Phase II of the small main-belt asteroid spectroscopic survey: A feature-based taxonomy". In: *Icarus* 158.1 (2002), pp. 146–177. DOI: 10.1006/icar.2002.6856.

[4] P Cambianica et al. "Quantitative analysis of isolated boulder fields on comet 67P/Churyumov-Gerasimenko". In: *Astronomy & Astrophysics* 630 (2019), A15. DOI: 10.1051/0004-6361/201834775.

[5] F Capaccioni et al. "Shapes of asteroids compared with fragments from hypervelocity impact experiments". In: *Nature* 308.5962 (1984), pp. 832–834. DOI: 10.1038/308832a0.

[6] NASA Goddard Space Flight Center. *OSIRIS-REx*. Flickr Album. URL: https://www.flickr.com/photos/gsfc/albums/72177720310727975/.

[7] AF Cheng et al. "AIDA DART asteroid deflection test: Planetary defense and science objectives". In: *Planetary and Space Science* 157 (2018), pp. 104–115. DOI: 10.1016/j.pss.2018.02.015.

[8] HC Connolly et al. "Initial Analysis of the OSIRIS-REx Sample from Asteroid Bennu: An Overview of the Petrography and Petrology". In: *LPI Contributions* 3040 (2024), p. 1281.

[9] M Delbo et al. "Alignment of fractures on Bennu's boulders indicative of rapid asteroid surface evolution". In: *Nature Geoscience* 15.6 (2022), pp. 453–457. DOI: 10.1038/s41561-022-00940-3.

[10] M Delbo et al. "Thermal fatigue as the origin of regolith on small asteroids". In: *Nature* 508.7495 (2014), pp. 233–236. DOI: 10.1038/nature13153.

[11] M Grott et al. "Macroporosity and grain density of rubble pile asteroid (162173) Ryugu". In: *Journal of Geophysical Research: Planets* 125.12 (2020), e2020JE006519. DOI: 10.1029/2020JE006519.

[12] D Haack et al. "Tensile strength of dust-ice mixtures and their relevance as cometary analog material". In: *Astronomy & Astrophysics* 642 (2020), A218. DOI: /10.1051/0004-6361/202037763.

[13] CW Hergenrother et al. "The design reference asteroid for the OSIRIS-REx Mission Target (101955) Bennu". In: *arXiv preprint arXiv:1409.4704* (2014). DOI: 10.48550/arXiv.1409.4704.

[14] ER Jawin et al. "Global geologic map of asteroid (101955) Bennu indicates heterogeneous resurfacing in the past 500,000 years". In: *Icarus* 381 (2022), p. 114992. DOI: 10.1016/j.icarus.2021.114467.

[15] ER Jawin et al. "Global patterns of recent mass movement on asteroid (101955) Bennu". In: *Journal of Geophysical Research: Planets* 125.9 (2020), e2020JE006475. DOI: 10.1029/2020JE006475.

[16] F Jourdan et al. "Rubble pile asteroids are forever". In: *Proceedings of the National Academy of Sciences* 120.5 (2023), e2214353120. DOI: 10.1073/pnas.2214353120.

[17] DS Lauretta et al. "Episodes of particle ejection from the surface of the active asteroid (101955) Bennu". In: *Science* 366.6470 (2019), eaay3544. DOI: 10.1126/science.aay3544.

[18] DS Lauretta et al. "OSIRIS-REx at Bennu: Overcoming challenges to collect a sample of the early Solar System". In: *Sample return missions*. Elsevier, 2021, pp. 163–194. DOI: 10.1016/B978-0-12-818330-4.00008-2.

[19] DS Lauretta et al. "OSIRIS-REx: sample return from asteroid (101955) Bennu". In: *Space Science Reviews* 212 (2017), pp. 925–984. DOI: 10.1007/s11214-017-0405-1.

[20] DS Lauretta et al. "The unexpected surface of asteroid (101955) Bennu". In: *Nature* 568.7750 (2019), pp. 55–60. DOI: 10.1038/s41586-019-1033-6.

[21] JJ Lissauer and I De Pater. *Fundamental Plantery Science - Physics, Chemistry and Habitability*. Cambridge University Press, 2013.

[22] T Michikami and A Hagermann. "Boulder sizes and shapes on asteroids: a comparative study of Eros, Itokawa and Ryugu". In: *Icarus* 357 (2021), p. 114282. DOI: 10.1016/j.icarus.2020.114282.

[23] T Michikami et al. "Boulder size and shape distributions on asteroid Ryugu". In: *Icarus* 331 (2019), pp. 179–191. DOI: 10.1016/j.icarus.2019.05.019.

[24] T Michikami et al. "Fragment shapes in impact experiments ranging from cratering to catastrophic disruption". In: *Icarus* 264 (2016), pp. 316–330. DOI: 10.1016/j.icarus.2015.09.038.

[25] NASA. *NEO Groups*. Ed. by Jet Propulsion Laboratory Center for Near Earth Object Studies. Accessed: 2024-05-20. URL: https://cneos.jpl.nasa.gov/about/neo_groups.html.

[26] KA Otto et al. "Surface roughness of asteroid (162173) Ryugu and comet 67P/Churyumov–Gerasimenko inferred from in situ observations". In: *Monthly Notices of the Royal Astronomical Society* 500.3 (2021), pp. 3178–3193. DOI: 10.1093/mnras/staa3314.

[27] QGIS.org. *QGIS Geographic Information System. Open Source Geospatial Foundation Project.* 2024. URL: http://qgis.org.

[28] AB Regberg. "OSIRIS-REx: Curating Samples from the Carbon rich Asteroid Bennu". In: *International Conference on Advances in Aerospace and Energy Systems*. 2024.

[29] B Rizk et al. "OCAMS: the OSIRIS-REx camera suite". In: *Space Science Reviews* 214 (2018), pp. 1–55. DOI: 10.1007/s11214-017-0460-7.

[30] B Rizk et al. *Spectral Interpretation, Resource Identification, Security, Regolith Explorer (OSIRIS-REx): OSIRIS-REx Camera Suite (OCAMS) Bundle*. urn:nasa:pds:orex.ocams, NASA Planetary Data System. 2019.

[31] CR Robin et al. "A comparative study of boulder morphology on small body surfaces". In: *LPI Contributions* 2851 (2023), p. 2256.

[32] H Roper, D Gallagher, K Elkins, et al. *OSIRIS-REx: X Marks the Spot - 2019 AGU Press Conference*. Credit: NASA/Goddard/University of Arizona. Accessed: 2024-05-22. 2019. URL: https://svs.gsfc.nasa.gov/13489/.

[33] A Sharma et al. "Effect of particle morphology on stiffness, strength and volumetric behavior of rounded and angular natural sand". In: *Materials* 14.11 (2021), p. 3023. DOI: 10.3390/ma14113023.

[34] NASA Planetary Data System. *PDS Small Bodies Node - Small Bodies Image Browser*. URL: https://sbn.psi.edu/pds/sbib/.

[35] T Szabó et al. "Reconstructing the transport history of pebbles on Mars". In: *Nature communications* 6.1 (2015), p. 8366. DOI: 10.1038/ncomms9366.

[36] KJ Walsh et al. "Craters, boulders and regolith of (101955) Bennu indicative of an old and dynamic surface". In: *Nature Geoscience* 12.4 (2019), pp. 242–246. DOI: 10.1038/s41561-019-0326-6.

[37] RA Yingst et al. "Quantitative morphology of rocks at the Mars Pathfinder landing site". In: *Journal of Geophysical Research: Planets* 112.E6 (2007). DOI: 10.1029/2005JE002582.

[38] K Zacny et al. “Asteroid mining”. In: *AIAA Space 2013 Conference and Exposition*. 2013, p. 5304. DOI: 10.2514/6.2013-5304.